

© 2010 Ankit Saharan

CHARACTERIZATION OF FUNCTIONALLY GRADED MATERIALS  
THROUGH FRACTAL GEOMETRY

BY

ANKIT SAHARAN

THESIS

Submitted in partial fulfillment of the requirements  
for the degree of Master of Science in Mechanical Engineering  
in the Graduate College of the  
University of Illinois at Urbana-Champaign, 2010

Urbana, Illinois

Adviser:

Professor Martin Ostoj-Starzewski

## Abstract

Functionally Graded Materials are the material systems whose properties vary spatially through the solid. These material systems are fairly new and though expensive to fabricate; they serve as excellent engineering materials for various applications. The material system we consider in this work is a metal-ceramic system, which can easily substitute for heat shielding tiles on the reentry space vehicles replacing the conventional ceramic tiles. This system while providing a structurally and thermally excellent heat shielding also reduces the weight penalty by introducing metal in the system without compromising on the strength. In this thesis we study the behavior and characteristics of the FGM in terms of fractals. There has been no prior literature on linking FGM and fractals. We characterize the interfaces between the two-phase FGM using fractals and estimate an *interfacial fractal dimension* for varying degrees of coarseness. Also, the variation in local fractal dimension as we move lengthwise (left to right) in the domain is characterized by a Fourier fit, and a simpler relation using a Beta function. Assuming an isotropic nature of both Titanium and Titanium Monoboride (TiB), pure shear tests are simulated using ABAQUS for coarseness level of 50, 100 and 200 under the Uniform Kinematic Boundary Condition (UKBC) and the Uniform Static Boundary Condition (USBC). The material response observed under both these BC's shows a high sensitivity of these systems to loading conditions. Furthermore, plastic evolution of Titanium grains assuming isotropic plastic hardening shows fractal plane filling behavior. Fractal dimensions of sets of plastic grains are calculated using the box counting method, and it validates our mechanical results, thus again showing high sensitivity of this material system to loading conditions.

## **Acknowledgements**

I would like to thank my advisor Professor Martin Ostoj-Starzewski for his unrelenting support and guidance during my research and study at University of Illinois. His perpetual enthusiasm and vision has inspired me. This research would not have been possible without his patience, which kept me going even when it was tough. I would also like to thank my research group colleague Mr. Jun Li for his invaluable help and advice throughout this research work.

Finally I would like to thank my family, Mr. Anil Saharan, Mrs. Rekha Saharan, Mr. Varun Saharan, and Ms. A.P. Shweta for always blessing me with their love and support.

## Table of Contents

<b>CHAPTER 1 - INTRODUCTION .....</b>	<b>1</b>
1.1 INTRODUCTION .....	1
1.2 MOTIVATION .....	3
<b>CHAPTER 2 – MODEL FORMULATION .....</b>	<b>6</b>
2.1 GEOMETRIC MODEL FORMULATION .....	6
2.2 MECHANICAL MODEL FORMULATION .....	8
<b>CHAPTER 3 – RESULTS .....</b>	<b>12</b>
3.1 GEOMETRICAL RESULTS.....	12
3.2 MECHANICAL RESULTS .....	21
<b>CHAPTER 4 – CONCLUSIONS .....</b>	<b>31</b>
<b>BIBLIOGRAPHY .....</b>	<b>33</b>

# CHAPTER 1 – INTRODUCTION

## 1.1 INTRODUCTION

Engineering materials involve a wide variety of systems, all of them offering various ways of classification and characterization according to various attributes like thermal properties, mechanical properties, electrical properties, and even their field of application. With an ever-increasing need for materials with higher functionality, it has been a known fact that single-phase homogenous materials have a limited scope of applicability. As a result, there has been a tremendous research effort in multi-phase heterogeneous material systems like traditional systems for example: alloys, compounds; and modern systems like composites and Functionally Graded Materials (FGM) to name a few.

The nature abounds in heterogeneous material systems; think of wood, bone, nacer, and bamboo to name a few. Man-made examples of heterogeneous material systems include particulate composites, fiber reinforced composites, concrete to name a few. These systems offer a wider scope of application with their generally superior mechanical, thermal or electrical material properties. Or, in other words, they fill the gap in scope which single-phase homogeneous material systems leave.

The FGM is a kind of material system in which the properties and/or composition of the structure changes quasi-continuously across the material domain. A basic unit of FGM is referred as a unit element. The unit element in itself would represent the composition, microstructure, and physical configuration of the FGM. Simplest of the FGM models in two different configurations can be illustrated in the Fig. 1.1. Figure 1.1(a) represents a so-called continuous gradation from one phase to another, and Fig. 1.1 (b) represents discontinuous or stepwise gradation from one phase to another [1]. Of course, the difference between these gradations hinges on how fine or how coarse the microstructure actually is.

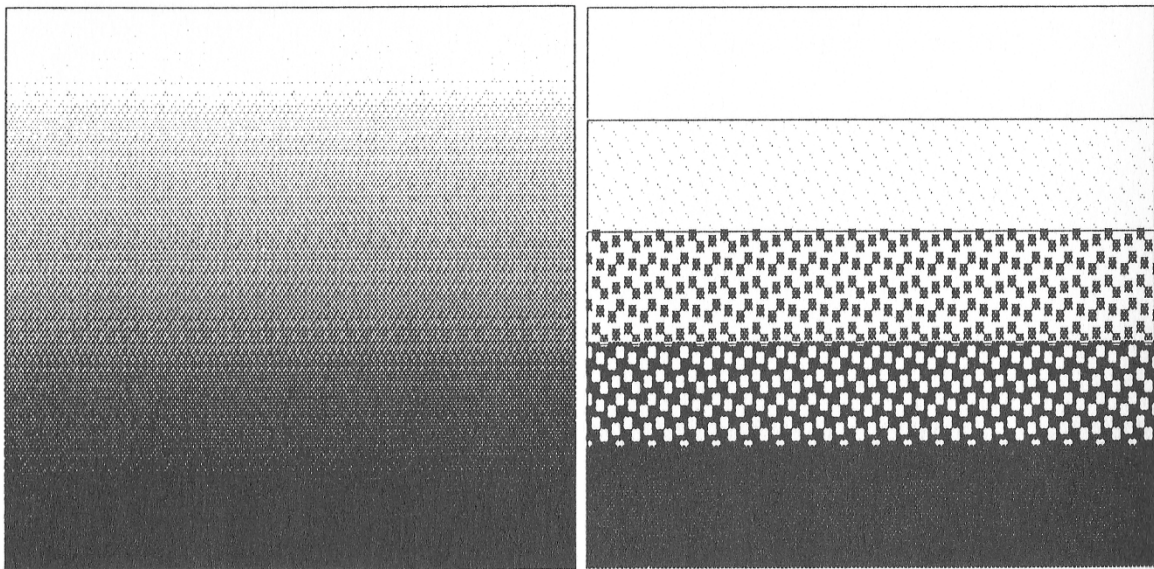


*Figure 1.1 (from left) (a) Continuous gradation; (b) Stepwise gradation [1]*

The continuous gradation is further illustrated in Fig. 1.2(a), where the composition varies linearly as a function of distance along in the spatial solid. Figure 1.2(b) represents how the composition changes in steps as a function of distance along in the spatial solid resulting in a layered microstructure of the Functionally Graded Material system.

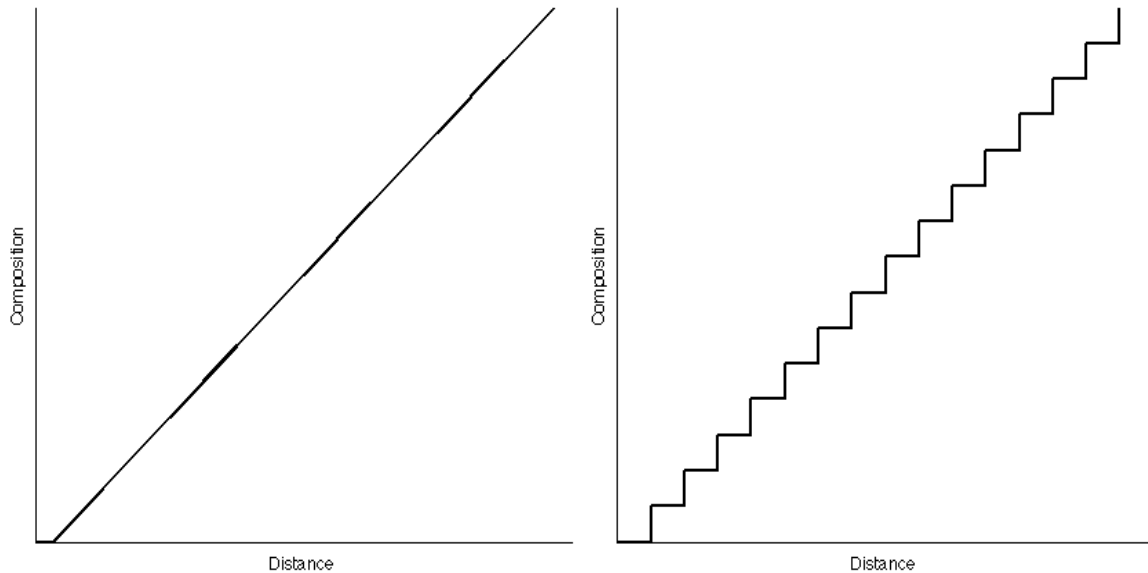
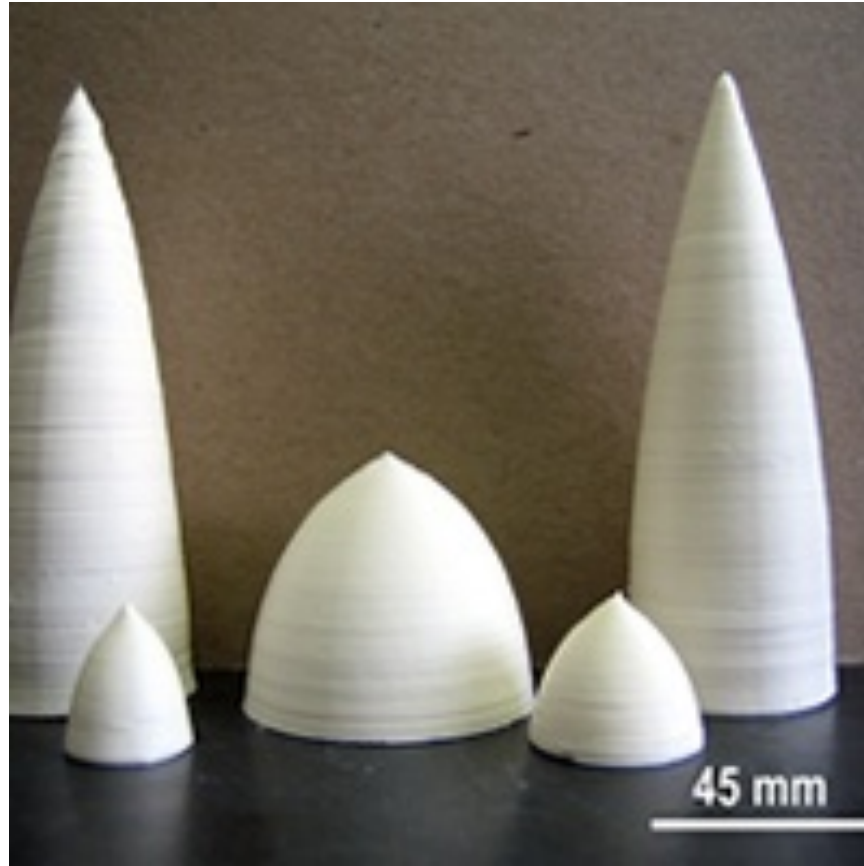


Figure 1.2 (from left) (a) Continuously Graded microstructure; (b) Layered microstructure

Various kinds of FGM material systems have been studied in the literature. Anandakumar *et al.* [2] studied thermal stress and failure analysis in functionally graded solid oxide fuel cells. Gunes and Aydin [3] studied elastic response of graded material system containing Metal (Al) and Ceramic (SiC) phases. The studies on FGM have been carried out in both the two-dimensional (2D) and 3D models, and for various loading cases including dynamic loading, low velocity impact loading, static elastic response, elastic-plastic transitions.

Reliability analyses of FGM with random constitutive mechanical properties have resulted in a non-linear power-law distribution of mechanical properties. The probabilistic-based reliability analyses were performed using Monte Carlo simulations, and mechanical properties distributions were estimated using Galerkin Finite Element and Newmark Finite Difference methods [4].

The FGM possess a wide application potential, ranging from the aerospace industry to biotechnology and energy sectors. The FGM are typically very expensive to process and very hard to control, thus limiting their applicability on a large scale. For space applications, especially for Reentry vehicle protection, thermal barrier coatings made of FGM are applicable. These thermal barrier coatings are also applicable for other applications including turbines, automobile, and boiler applications [1,7].



*Figure 1.3 FGM components consisting of metal-ceramic phases [8]*

Figure 1.3 illustrates the example of components fabricated using FGM materials for aerospace applications. Various other applications of FGM also include in the Energy Sector. Energy conversion systems like Solar Receiver system, and fuel cell have great scope and utility for Functionally Graded Materials [1].

Section 1.2 would discuss the objective and scope of the work. Chapter 2 mainly deals with the Problem formulation for both geometrical and mechanical interpretation. Chapter 3 will present the results and analysis of the problem both geometrically and mechanically. Chapter 4 would cover the conclusions and future scope of this research work.

## **1.2 MOTIVATION**

The Functionally Graded Materials (FGM) as we see are considered great engineering materials worth spending financial resources, time and effort to further their research and development. This is primarily because, in general, they have far superior properties to those of their conventional counterparts like metals, ceramics, polymers etc. Since, the FGM are employed or about to be employed in many



critical applications like space, nuclear energy etc, understanding their failure mechanisms is of paramount importance.

Of many studies performed on failure of the FGM, we review the select few which relate to our own research. C.S. Lee et al. [9] performed three-dimensional analysis to estimate residual stresses in multilayered FGM samples using Finite Element Analysis. They applied the von Mises and maximum stress criterion to predict failure and they concluded that the first of these is more accurate in predicting crack location. The micromechanical based approach has also been applied to FGM used for heat-shielding applications [10], where using plane stress loading, a fracture criterion was derived which takes into account plastic deformation and brittle state stress. Buckling and postbuckling behavior of FGM plates was also studied along with piezoelectric actuators [11], where the effect of compressive buckling and thermal buckling on postbuckling load deflection curves was studied [11].

An elastic-plastic analysis was performed on FGM under thermal loading by Mahmoud *et al.* [12] who studied the effect of thermal loading on 1D and 2D FGM. The analysis assumed model based on rule of mixtures, and numerical analysis was performed on the same using Finite Element Technique. In [13] J. Aboudi *et al.* studied thermoplastic response for two-dimensional Functionally Graded Materials; the effect of microstructure and plasticity on free edge inter-laminar stresses was studied and it concluded inability of homogenization to accurately represent the micro structural effects on the free edge.

Most of the above approaches require some estimation or measurement of stresses/strains on the FGM to determine the failure of the material or even determine the plastic flow in the material. The measurement of these stresses/strains can be quite complicated requiring often expensive and time consuming procedures, which are necessary to even analyze the plastic deformation. In this study, we investigate the evolution of plastic grains in the FGM using a geometric concept not yet applied in this area: fractals. As is well known, there are numerous interpretations of fractals in the literature. Fractals have been found to accurately represent randomness of geometry in nature. Fractals can be used to represent amazingly accurate clouds, landscape topology, diffusion of particles. Quoting from Mandelbort [5]: “A fractal is a shape made of parts similar to the whole in some way”. Overall, there has been very little research on fractals in elastic-plastic problems. Fractals during the evolution of plastic grains have been very recently studied on both elastic/perfectly plastic and elastic/plastic-hardening responses [14,15]. The grains were assumed to be isotropic in nature and some amount of random noise was introduced in elastic and plastic material properties. Very nice fractal behavior was observed in both the studies, which show that fractals can be a very good measure to determine the plastic behavior in a material.

The fractal dimension can be as useful measure to determine plasticity or yielding of a material as Von Mises Stress. In addition, Von Mises stress is tricky to measure experimentally, while fractals can be

observed on the plastic grains on image. In this study we consider a common FGM system of Titanium-Titanium Monoboride (Ti-TiB). The system assumed in this study is one-dimensional FGM. There have been many studies performed on this material system as will be indicated in section 2.2.

To our knowledge this will be a first ever attempt to measure the fractal dimension of Phase Interfaces in the two phases FGM. Also, this will also be a first ever attempt to measure fractal dimension of evolving plastic grains under both kinematic and static boundary conditions in plastic hardening FGM model.

## CHAPTER 2 – MODEL FORMULATION

### 2.1 GEOMETRIC MODEL FORMULATION

The FGM microstructure is modeled on a chessboard model. The black and white boxes on the chessboard represent two phases in the FGM material system. We refer from here on the chessboard to a field domain of size  $L$ , having black and white grains. Starting from the left boundary of the domain, the probability of the black grains equals 100% and decreases linearly to 0% as we approach the right boundary of the domain. Similarly, the white grains have a 100% probability starting from right boundary of the domain and decrease to 0% as we approach the left boundary of the domain.

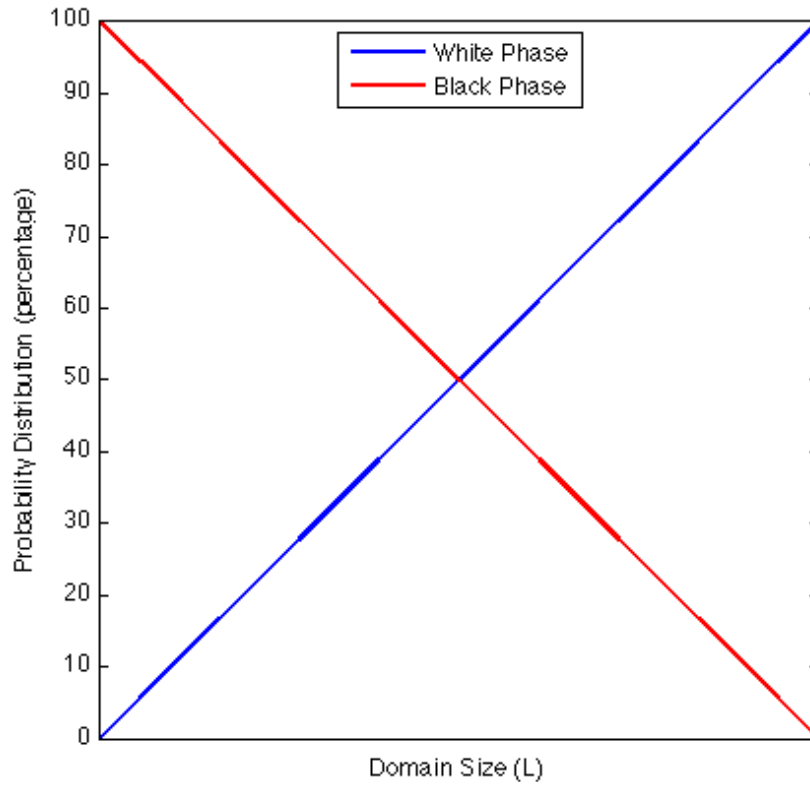


Figure 2.1 Probability Distribution of black and white material phases

Given that this model of an FGM is non-deterministic, it is taken as a random medium  $B = \{B(\omega); \omega \in \Omega\}$ , where  $B(\omega)$  represents a specific realization, with  $\omega$  being an elementary event of the underlying sample space  $\Omega$ . Fig. 2.2 gives examples of  $B(\omega)$  at different coarseness levels within the same size domain. At this point, we define *coarseness* as the quality of FGM being composed of relatively large grains. In our model, the higher is the coarseness, the lower is the actual number describing it.

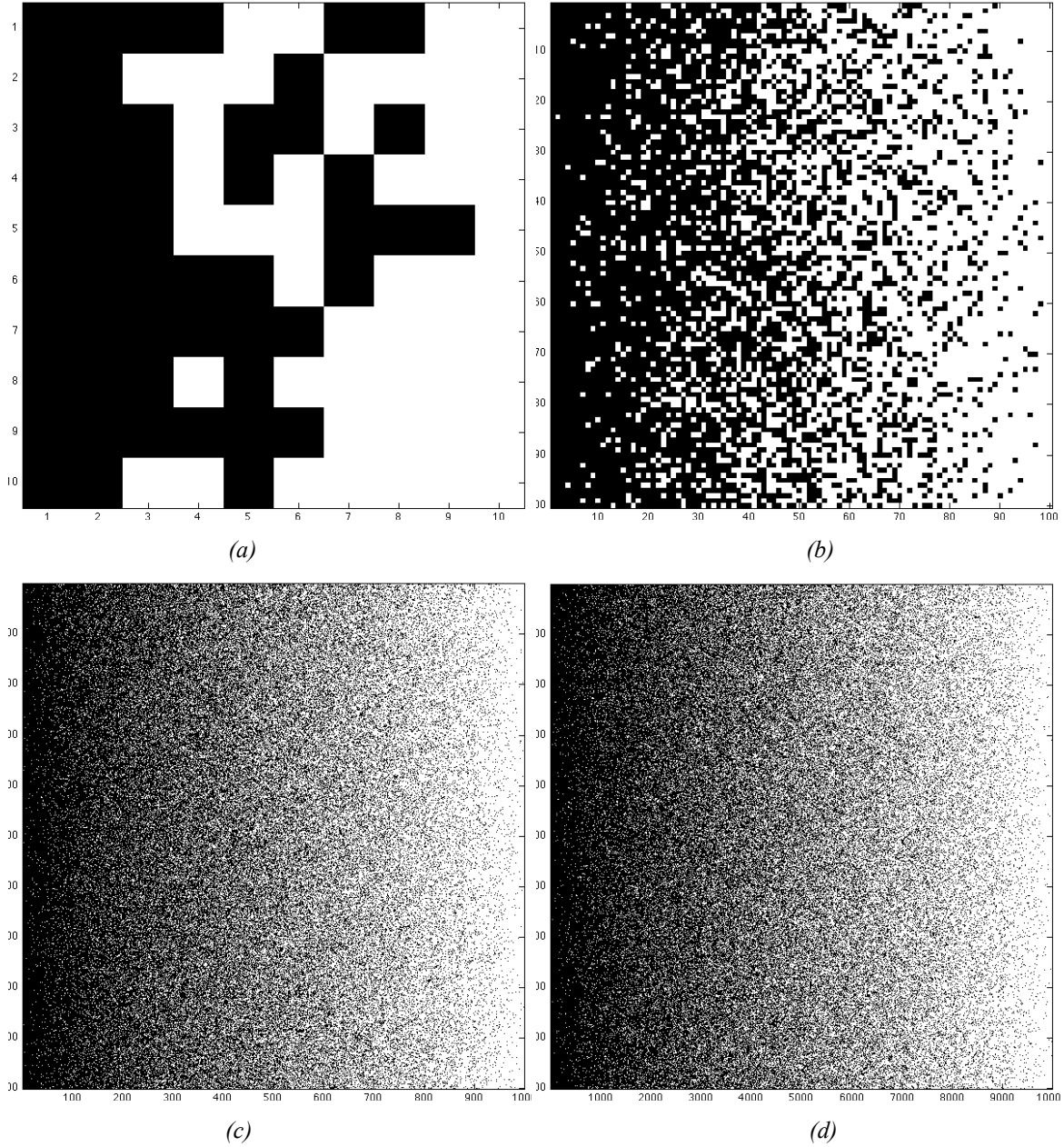


Figure 2.2 (a) coarseness of 10; (b) coarseness of 100; (c) coarseness of 1,000; (d) coarseness of 10,000.

Furthermore, we will be interested in the interface edges between the black and white phases. Since these interface edges appear randomly throughout the domain, we observe dense edge structures in the middle of the domain, as that is the place where the coexistence of black and white phases (or their mixing) is the highest with  $P(\text{Black}, \text{White}) = \{0.5, 0.5\}$  (probability distribution of each phase). Figure 2.3 gives so-called *edge plots* for the coarseness levels of 100 and 1,000.

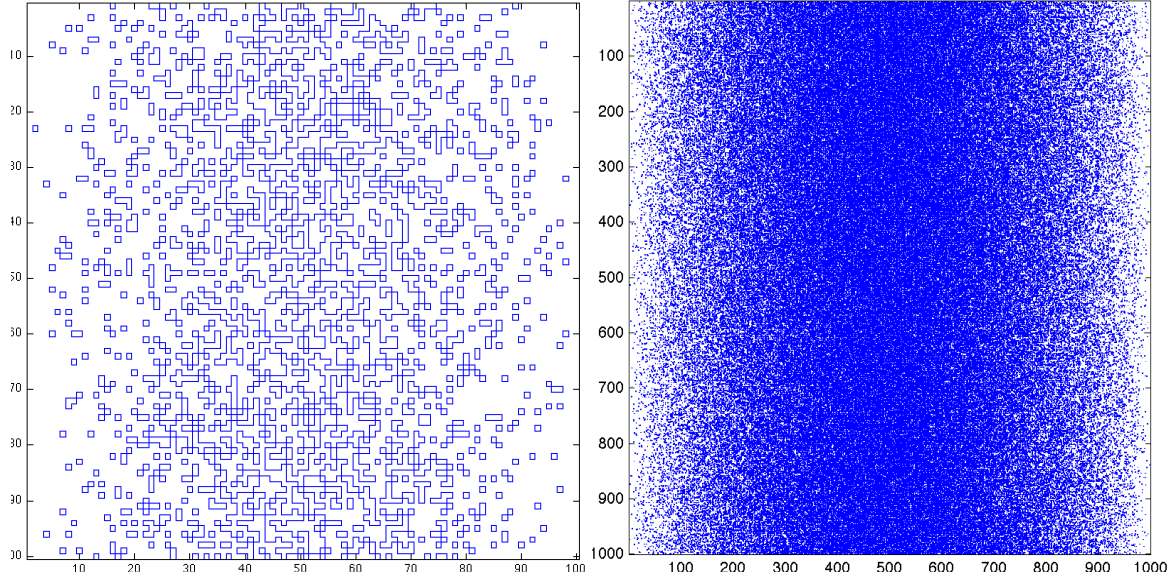


Figure 2.3 (from left) (a) edge plot of coarseness 100, corresponding to Fig. 2.2(b); (b) edge plot of coarseness 1,000, corresponding to Fig. 2.2(c)

## 2.2 MECHANICAL MODEL FORMULATION

The material system we consider in this work is the Titanium -Titanium Monoboride (TiB) FGM. There has been considerable amount of research on this material system in the literature. Rule of mixtures, modified rule of mixtures have been applied to construct numerical model of this two-phase material system [19-23]. This material system has tremendous scope in armor-ballistic applications, as TiB, a ceramic can sustain damage from high velocity projectiles. The other phase, Titanium, being a softer material may serve as a containment unit [21]. Another application of this system is in the automobile industry. The exhaust valve of automobiles made from this material system has exhibited enhanced durability and reliability [24]. Yet another possible application of this system is the heat shields of space vehicles. During the reentry into the earth's atmosphere, surfaces of these shields are exposed to massive amounts of friction with the earth's atmosphere leading to significant heating of the exposed surface. Conventionally ceramic tiles are used for protection as these materials provide excellent heat protection, though at some weight penalty. As a stepping-stone in this direction, in this study we research such an FGM system, as the TiB phase, just like any ceramic, would provide excellent heat shielding while the Titanium phase would reduce the weight cost while maintaining the structural integrity.

Titanium being a softer material, it undergoes plastic deformation, and the TiB being a ceramic, remains elastic throughout. However, the spatial patterns associated with the phenomenon seem to be unknown as yet. Overall, the response of FGM made of Titanium-TiB is expected to have an intermediate response between its two constituent phases as shown in Fig. 2.4.

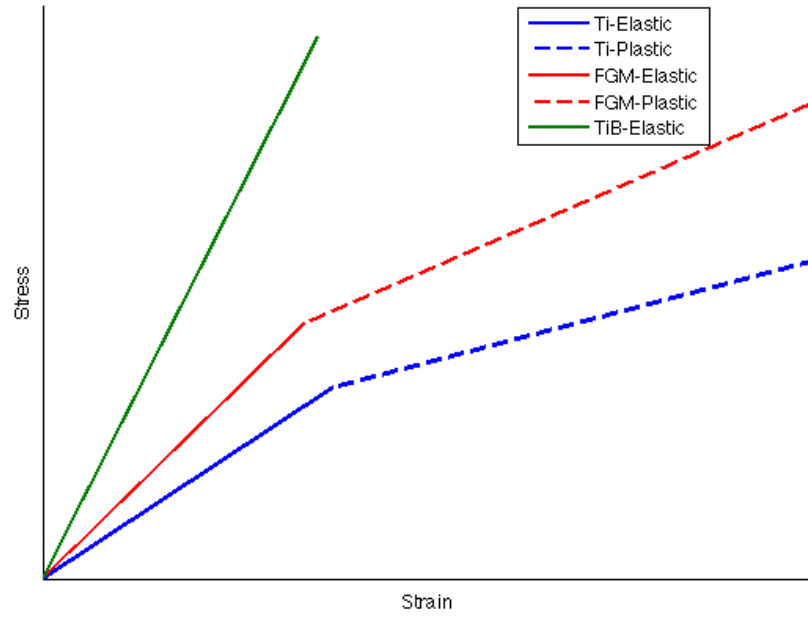


Figure 2.4 Illustration of the stress-strain response of the FGM and its two constituent phases

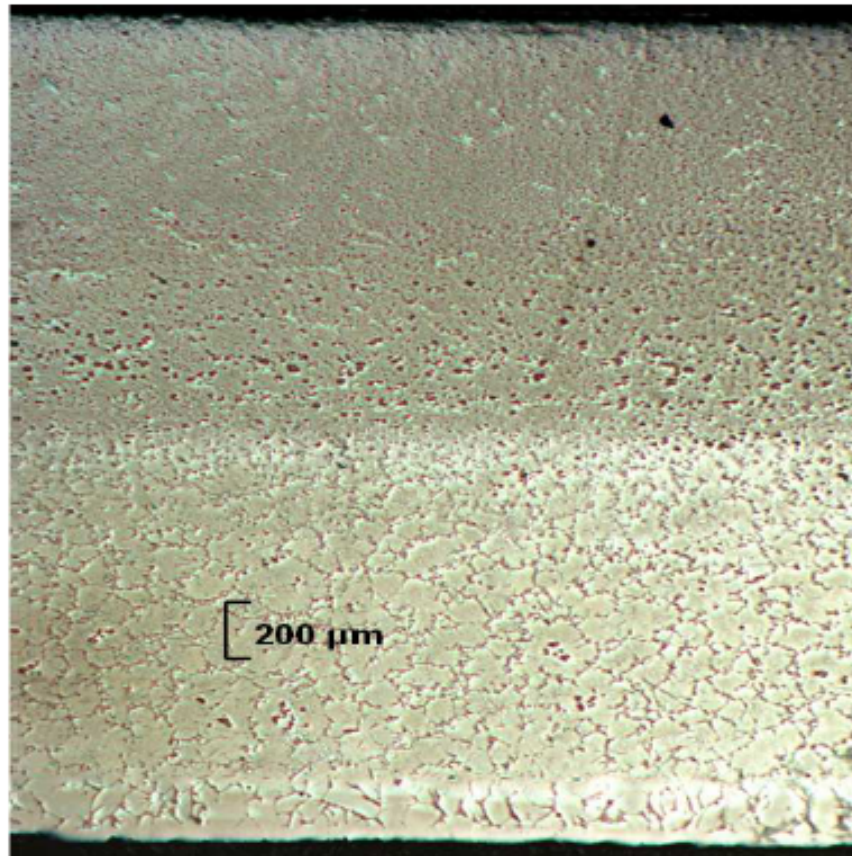


Figure 2.5 Microscopic view of Titanium-TiB FGM. Titanium region near the top; TiB region near the bottom [23]

Essentially, Titanium is an anisotropic material. It is a hexagonal closed packed (HCP) crystal at room temperature. TiB on the other hand is a hard brittle ceramic. The crystal structure of TiB is B27 class orthorhombic [23]. For our model constructed, we have assumed isotropic response for Titanium and TiB, with Titanium undergoing isotropic plastic hardening beyond its yield point. The material properties we have taken for Titanium is for the A70 commercially available pure titanium. Its properties are given in Table 2.6.

Property	Value	Units
Young's Modulus	104	GPa
Poisson's Ratio	0.3	
Yield Strength	482.633	MPa
Density	4512	Kg/mm <sup>3</sup>

Table 2.6 Material Properties of commercially pure Titanium (A70) at room temperature [17,18,23,25]

The plastic deformation in A70 follows a parabolic relation beyond its yielding point. The relation depends on the Titanium grain size as well, and is given in equation 2.1 [18],

$$\sigma = \sigma(0) + h\sqrt{\epsilon} \quad (2.1)$$

$\sigma$  is the flow stress,  $\sigma(0)$  is the intercept,  $h$  is the strain hardening coefficient, and  $\epsilon$  is the true strain.

The values of the above parameters for A70 are as follow,

$$\sigma(0)=510 \text{ MPa}; h=833 \text{ MPa} [18].$$

The properties of TiB are given in Table 2.7.

Property	Value	Units
Young's Modulus	370	Gpa
Poissons Ratio	0.4	
Density	4630	Kg/mm <sup>3</sup>

Table 2.7 Material properties of TiB at room temperature [23]

In the model we formulate we apply a pure shear load using UKBC (Displacement) and USBC (traction) for system coarseness of either 50, 100 or 200. We assume plane strain condition. We try to achieve the classical RVE response from our material system, and observe the behavior of the model as we increase the coarseness of our model.

The UKBC is applied on our model according to

$$u = \epsilon^0 \cdot x, \quad \forall x \in B \quad (2.2)$$

and, more specifically, via pure shear loading

$$\epsilon_{11}^0 = \epsilon_{22}^0 = 0, \quad \epsilon_{12}^0 = \epsilon_{21}^0 = \epsilon \quad (2.3)$$

The USBC is applied according to

$$t = \sigma^0 \cdot n, \quad \forall x \in B \quad (2.4)$$

with

$$\sigma_{11}^0 = \sigma_{22}^0 = 0, \quad \sigma_{12}^0 = \sigma_{21}^0 = \sigma \quad (2.5)$$



## CHAPTER 3 – RESULTS

### 3.1 GEOMETRICAL RESULTS

We generated 2-D FGM material system as explained in Section 2.1 on various coarseness levels. Although the probability distribution of either phase is varying linearly across the material domain, the FGM has a fine structure at smaller scales down to the grain level, and, to the spatially inhomogeneous statistics, it is too irregular to be easily described by a traditional Euclidean geometric language. Clearly, it is statistically self-similar in the  $y$ -direction, and it follows that the fractal dimension of some set associated with this FGM is greater than its topological dimension and non-integer. Thus, to characterize the FGM, we would like to assess its fractal characteristics. Henceforth, we focus on the system of black-and-white interfaces, henceforth referred to as an *edge set*. In other words, neither the white-white nor the black-black interfaces contribute to the edge set.

Clearly, the edge sets are sparse close to the left and right boundaries of the FGM, but quite dense in the middle. In this thesis we are only able to plot the edge sets for coarseness not exceeding 1,000 due to a limited computing power available. Figure 2.3 represents these edge sets for coarsenesses 100 and 1,000.

Now, we measure the fractal dimension  $D$  of these edges on various sizes of domain and study the variation in this dimension across the solid. Fractal dimension of the entire domain in the  $x$ -direction is calculated according to the relationship in equation 3.1.

$$R = N^D \quad (3.1)$$

$$R = \frac{X_n}{2}$$

Where,  $X_n$  is the number of edges in the domain, and  $N$  is the size of the system. We divide the number of edges by a factor of 2, since we are moving across the FGM length-wise (left to right). We further express the fractal dimension by

$$D = \frac{\text{Log}_{10}(R)}{\text{Log}_{10}(N)} \quad (3.2)$$

For example, for one simulation of system size of 10, we calculate,

$$R = \frac{57}{2} = 28.5$$

$$D = \frac{\text{Log}_{10}(28.5)}{\text{Log}_{10}(10)} = 1.4548$$

We call thus calculated fractal dimension  $D$  an *interfacial fractal dimension*. It is analogous to the fractal dimension of the Triadic Koch Curve [5]. Since the domain coarseness of 10 is too small to speak

in a meaningful way about fractals, we see a high noise in the estimation of  $D$ , Fig. 3.1. But, as we go to finer systems we observe that this noise decreases. The following set of figures illustrates this effect.

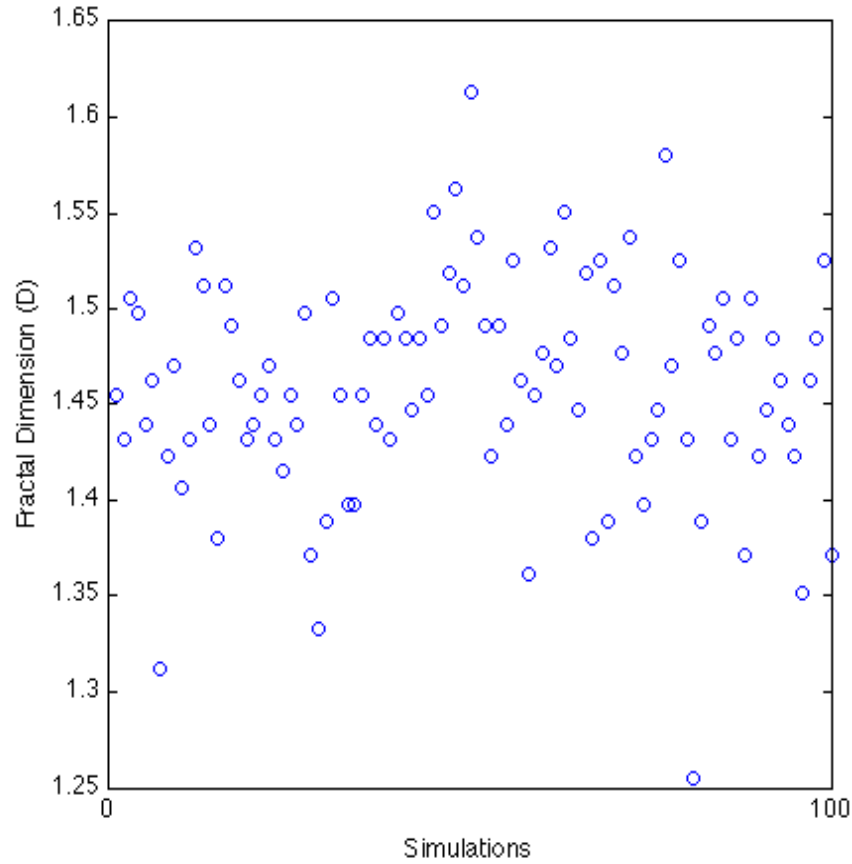


Figure 3.1 Noise in Fractal Dimension ( $D$ ) over 100 simulations in system size of 10

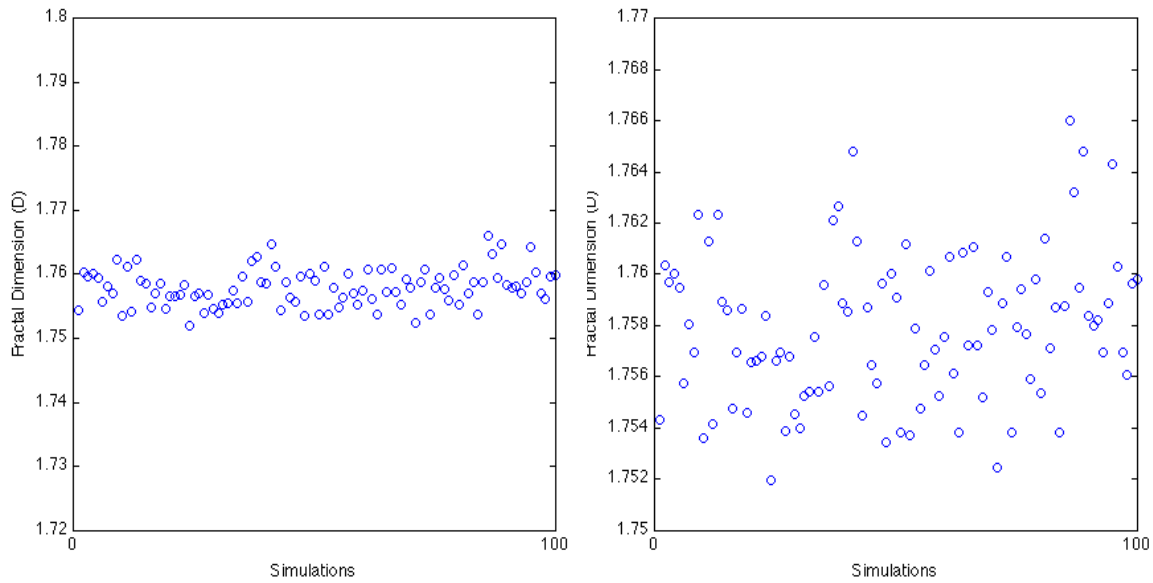


Figure 3.2 (from left) (a) Noise in estimation of  $D$  for coarseness of 100; (b) Same plot at greater resolution

Figure 3.2 illustrates this effect in domain coarseness of 100. Again, according to plots above the value of fractal dimension stabilizes as we move to higher a higher coarseness level of 100. From the plot in Fig. 3.2, the fractal dimension varies between  $1.75 < D < 1.77$  with a maximum value of  $D$  being 1.7660 and a minimum being 1.7520.

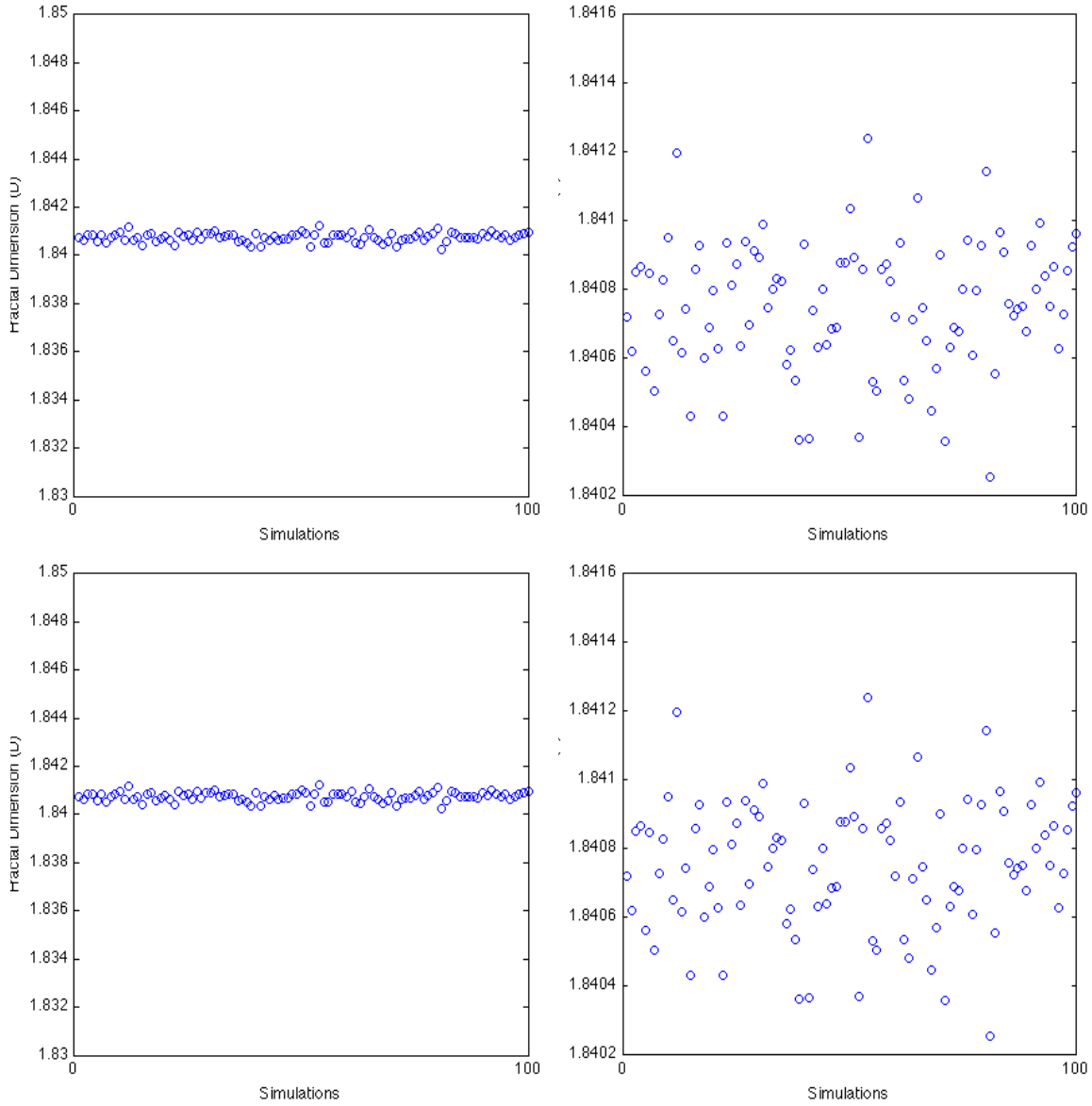


Figure 3.3 (from left) (a) Noise in estimation of  $D$  for coarseness of 1,000; (b) Same plot at greater resolution

Figure 3.3 illustrates the effect in system of coarseness 1,000 as the value of fractal dimension further stabilizes over 100 simulations as we move higher into the system order with dimension varying as  $1.840 < D < 1.842$ . The maximum value of  $D$  noted in this domain was of value 1.8412 and the minimum value was noted to be 1.8403.

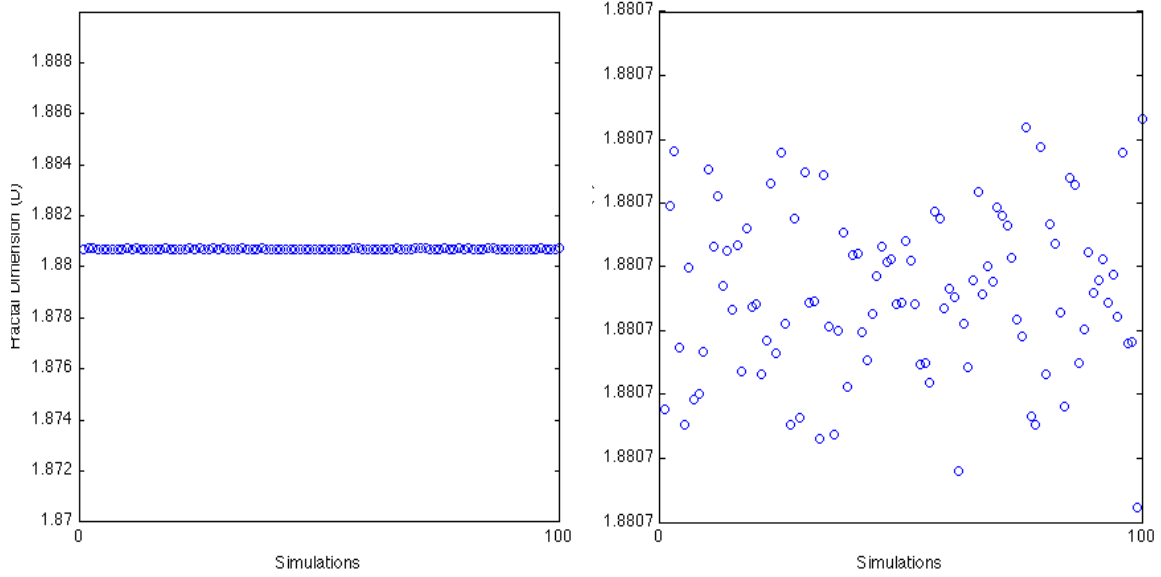


Figure 3.4 (from left) (a) Noise in estimation of  $D$  for coarseness of 10,000; (b) Same plot at greater resolution

As we see in Fig. 3.4, the value of fractal dimension further stabilizes as we move to domain coarseness of 10,000 over 100 simulations. The value of fractal dimension in this system can be averaged as  $D \sim 1.8807$ . As the maximum value of  $D$  noted for this system is 1.88073313 and the minimum value of  $D$  for the same system was noted as 1.88067238. This was the maximum system we could plot with the computing resources at disposal. We calculated the fractal dimension for various levels of coarseness and the maximum system size we tested had coarseness of 19,001. The fractal dimensions for various levels of coarseness have been listed in Table 3.5. The fractal dimension up to system size of 500 has been averaged over 100 simulations. The fractal dimension up to system size of 10,000 has been averaged over 10 simulations. The fractal dimension of system size up to 19,001 corresponds to one simulation.

Coarseness of FGM	Interfacial Fractal Dimension
10	1.459328817
50	1.710635642
100	1.757886781
500	1.822756529
1000	1.840748953
5000	1.870978452
10000	1.880705808
15001	1.88573187
19001	1.888491704

Table 3.5 System coarseness and corresponding Interfacial Fractal Dimension

We further represent the tabulated data in Table 3.5 in Fig. 3.6. We can observe that the slope or the interfacial fractal dimension reaches value of  $D \sim 1.889$  for higher levels of coarseness. The trend in the plot shows that the value of the interfacial fractal dimension stabilizes as we go to higher orders of coarseness. The red line in the plot represents slope of 1.889. The bubbles on the plot represent the data points given in Table 3.5.

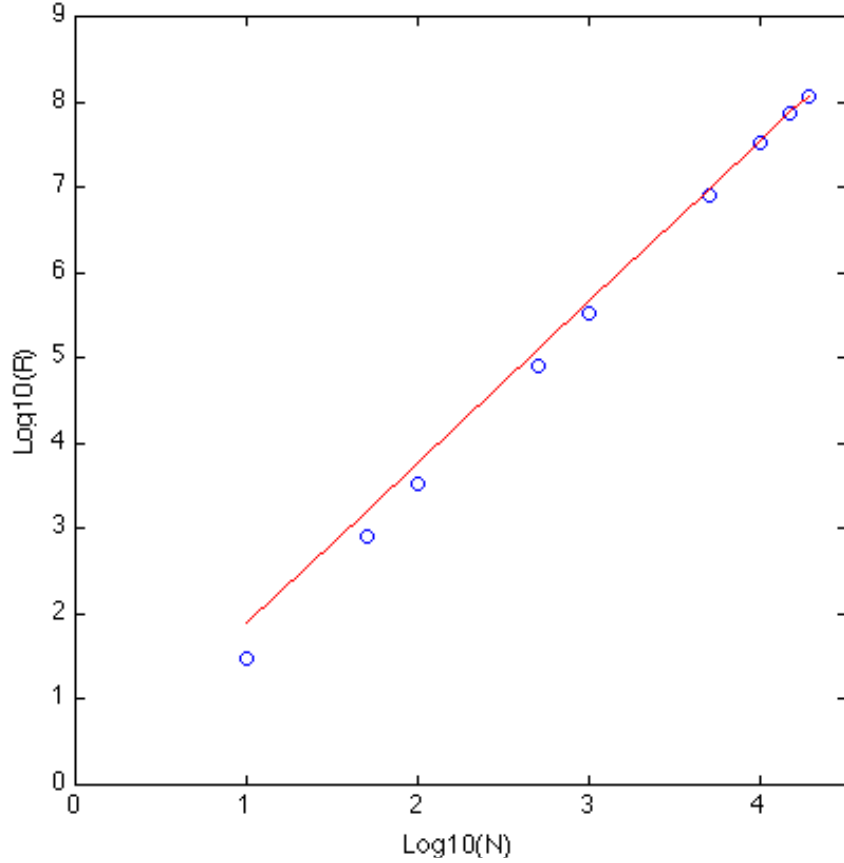


*Figure 3.6 Log curve of R and N (domain coarseness)*

Now, we further look at how this interfacial fractal dimension is varying lengthwise and widthwise across the solid. Now, for the sake of characterizing and observing the distribution of the interfacial fractal dimension as we move on, we consider a domain of coarseness 1,000. The interfacial fractal dimension is estimated locally using equation 3.2 given earlier in this section. The edges or interfaces are counted locally as a function of their position as we move across the solid both lengthwise and widthwise. Figure 3.7 represents how this interfacial fractal dimension is varying across the system.

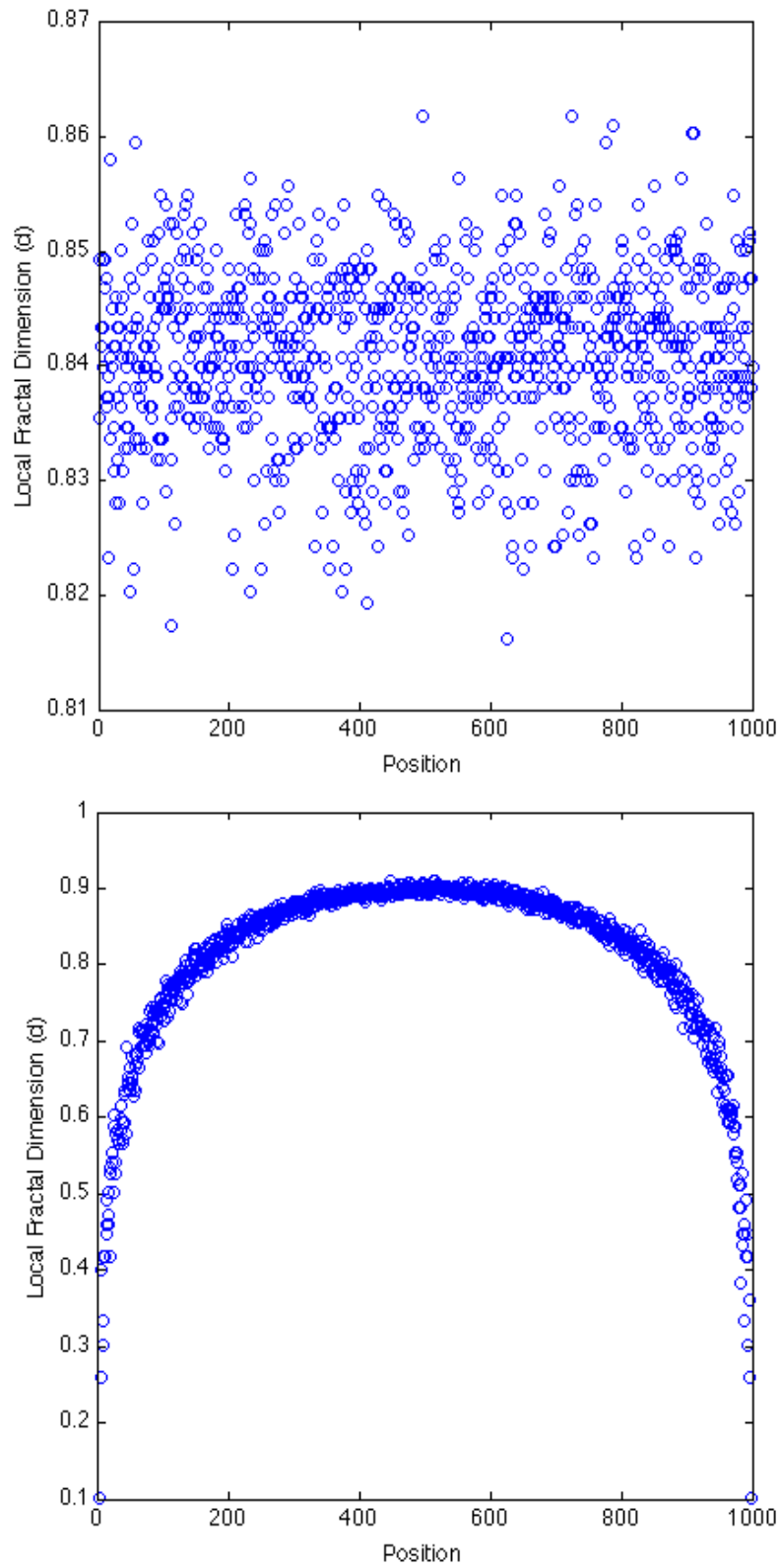


Figure 3.7 (from top) (a) Variation in  $d$  widthwise (top-bottom); (b) Variation in  $d$  lengthwise (left-right)

It is evident from Fig. 3.7(a) that the variation in local fractal dimension does not show any trend as we move through the solid widthwise. However, a clear trend can be discerned from Fig. 3.7(b), where the variation in local fractal dimension is plotted as a function of position in the solid. We now go ahead and characterize this trend by curve fitting. The Fourier fit and Beta function fit were applied to characterize this trend. The Fourier fit was applied using MATLAB curve fit toolkit and the results are given in Fig. 3.8.

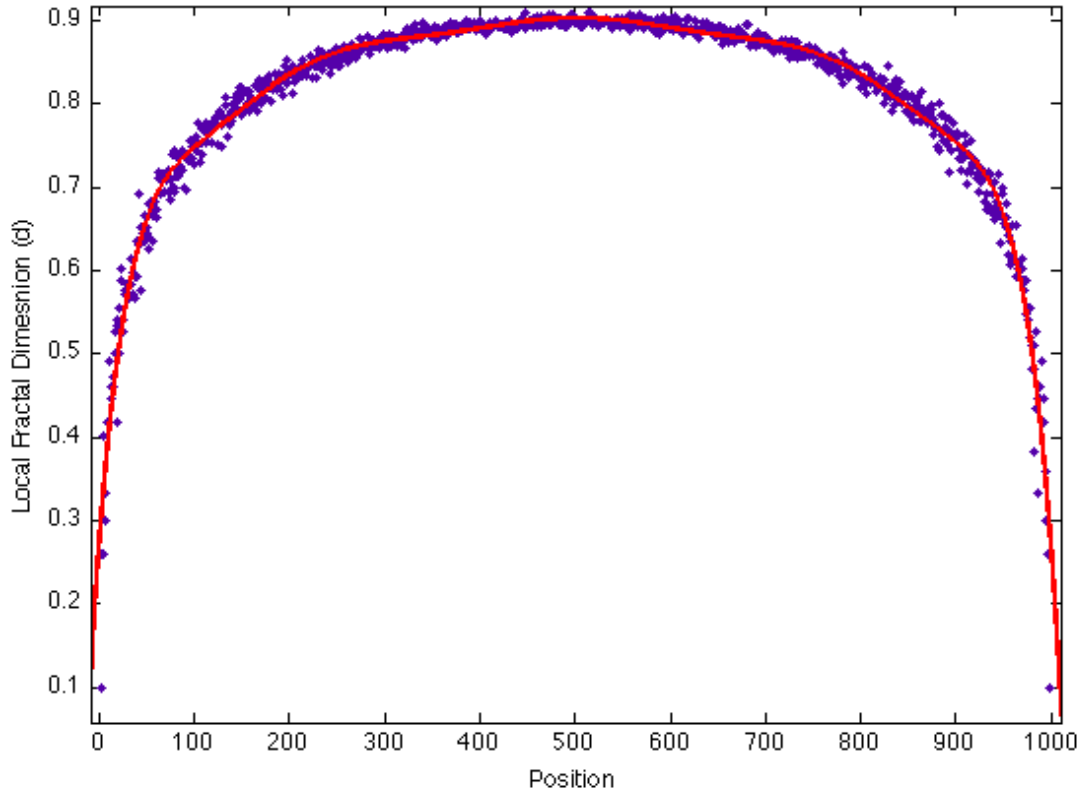


Figure 3.8 Fourier fit applied to variation in  $d$

The red line on the plot in the figure above represents the fit. The equation for the fit above with its values of coefficients is

$$\begin{aligned}
 f(x) = & a_0 + a_1 \cos(\omega x) + b_1 \sin(\omega x) + a_2 \cos(2\omega x) + \\
 & b_2 \sin(2\omega x) + a_3 \cos(3\omega x) + b_3 \sin(3\omega x) + \\
 & a_4 \cos(4\omega x) + b_4 \sin(4\omega x) + a_5 \cos(5\omega x) + b_5 \sin(5\omega x)
 \end{aligned} \tag{3.3}$$

$x$  is normalized by mean 500 and std 288. The values of the coefficients of the Fourier fit are

$$a_0 = -3.897e + 06; \omega = 0.2666$$

$$a_1 = 6.525e + 06; b_1 = -1833$$

$$a_2 = -3.781e + 06; b_2 = 2098$$

$$a_3 = 1.451e + 06; b_3 = -1182$$

$$a_4 = -3.331e + 05; b_4 = 350.5$$

$$a_5 = 3.473e + 04; b_5 = -43.7$$

The Fourier is a reasonable fit and the residuals are plotted in Fig. 3.9. The plot shows that the residuals are very small, though they are noisy at the boundaries.

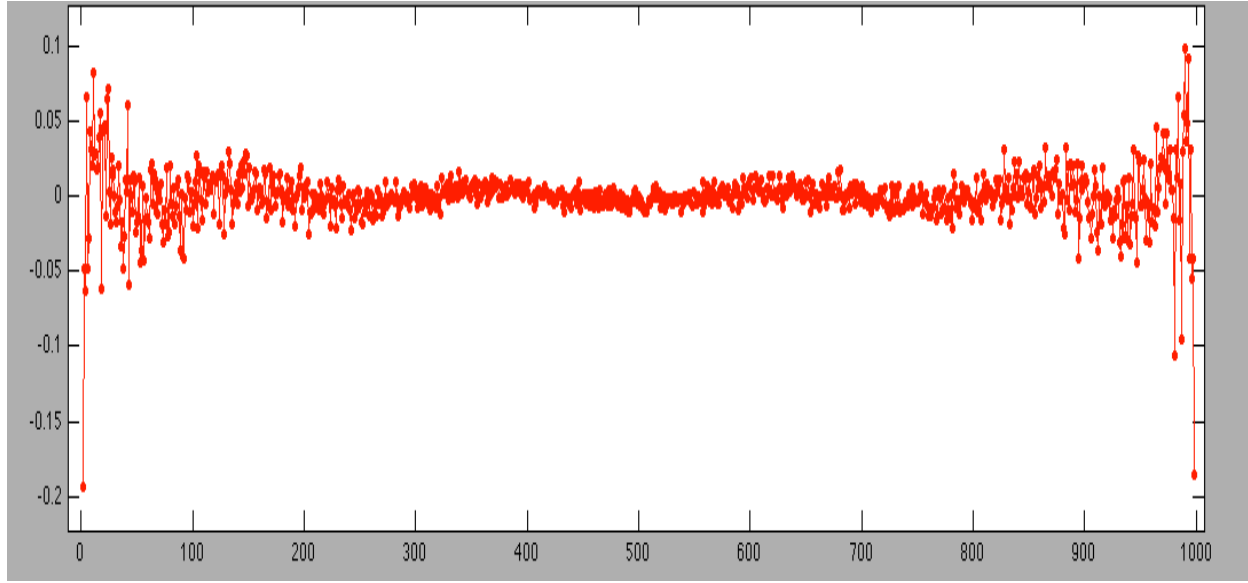


Figure 3.9 Residuals of the Fourier fit (y axis) v/s position

Another fit is applied to the trend observed in Fig. 3.7(b) using the Beta function, see the solid red line in Fig. 3.10(a). The corresponding residuals are plotted in Fig. 3.10(b). The beta function  $B(x,y)$  is [6]

$$B(x,y) = \frac{\Gamma(x)\Gamma(y)}{\Gamma(x+y)} = \int_0^1 t^{x-1} (1-t)^{y-1} dt \quad (3.4)$$

$\Gamma(z)$  is the so-called Gamma function

$$\Gamma(z) = \int_0^\infty t^{z-1} e^{-t} dt \quad (3.5)$$



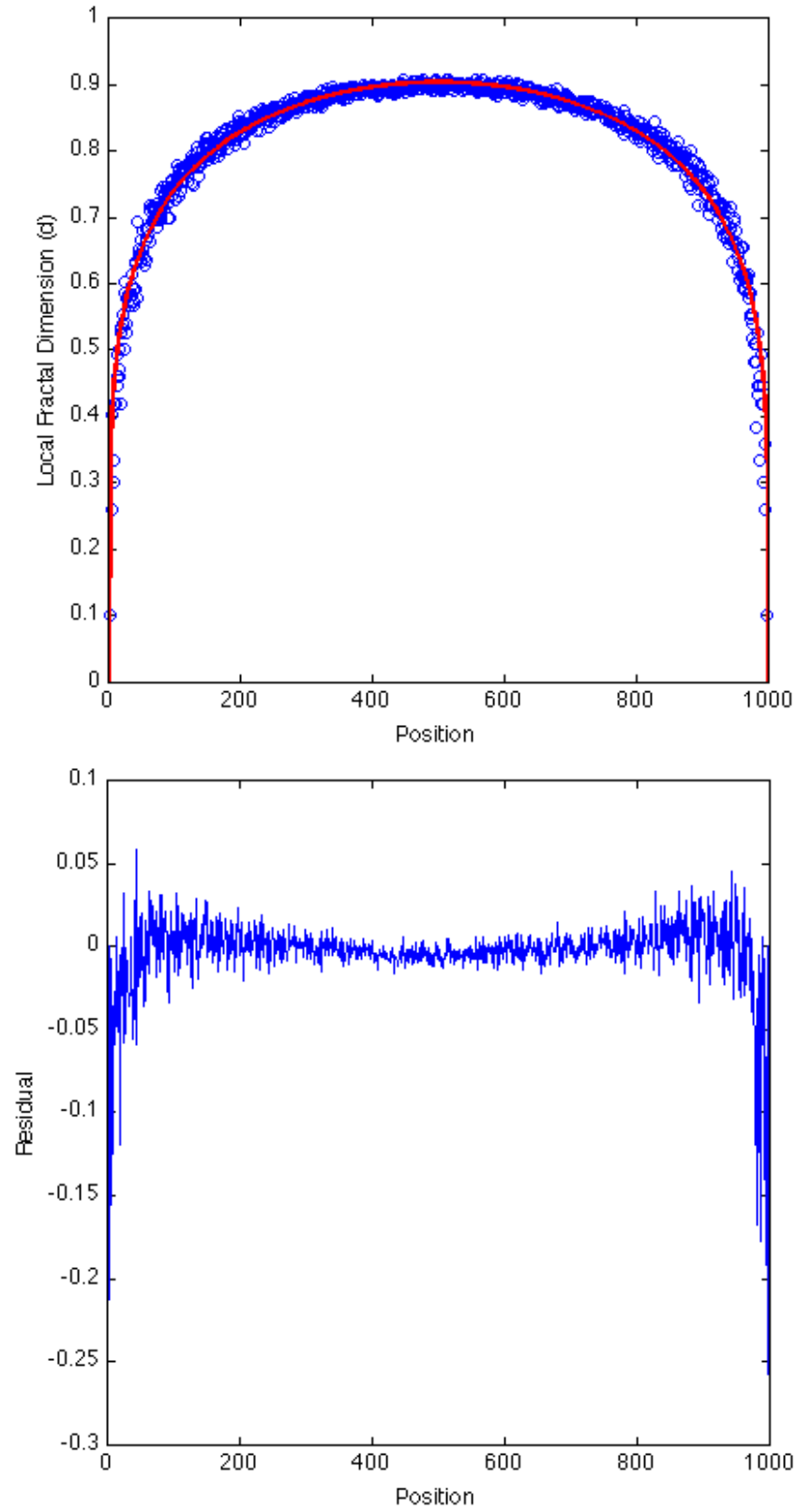


Figure 3.10 (from top) (a) Beta Function applied to the variation in  $d$ ; (b) Residual of Beta function v/s position

The equation representing this fit is

$$f(x) = \frac{x^{\alpha-1}(1-x)^{\beta-1}}{B(\alpha,\beta)} C \quad (3.6)$$

Where  $\alpha$  and  $\beta$  equal 1.692, and  $C=0.8129$ . The equation 3.6 represents a much simpler function and a fit that is easier to represent than that of equation 3.3. The residual plot in Fig. 3.10(b) also shows considerable noise in the residuals at the boundaries, which is analogous to the residual behavior of the Fourier fit given in Fig. 3.9.

### 3.2 MECHANICAL RESULTS

We now discuss the results of the mechanical simulation of the problem we setup in Section 2.2. We apply pure shear loading through UKBC and USBC on domain with coarseness of 50, 100 and 200; see Fig. 3.11.

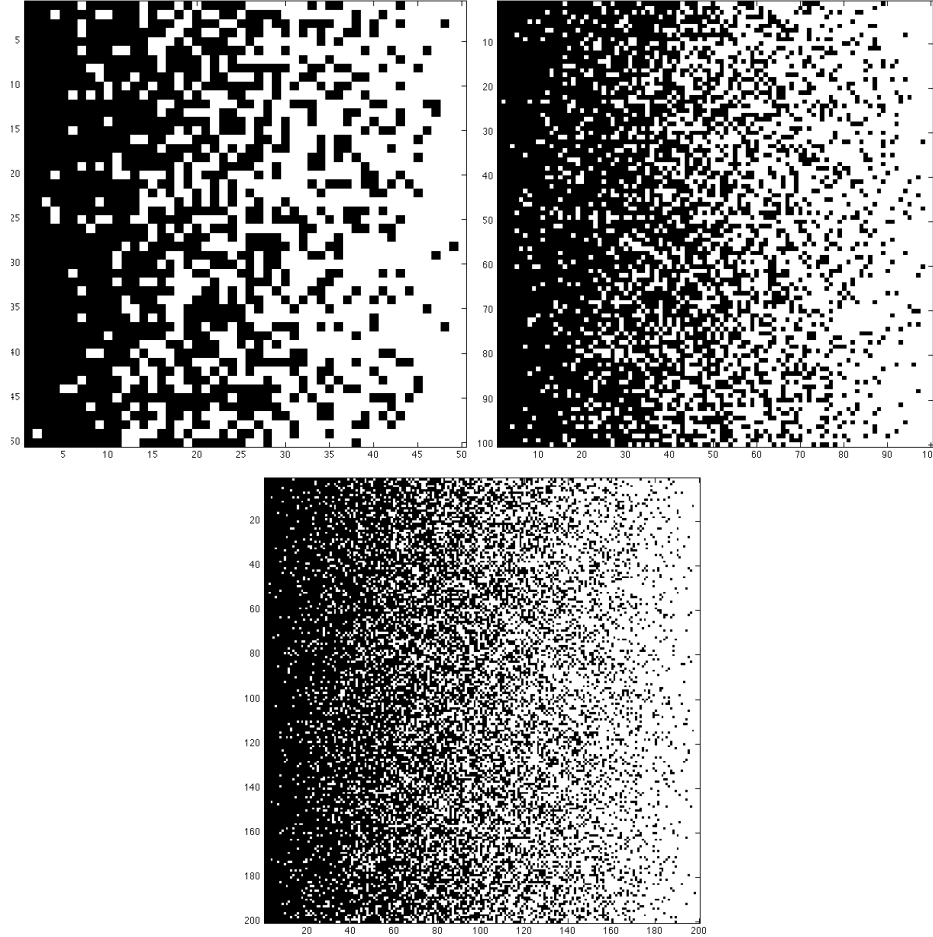


Figure 3.11 (from top left clockwise) FGM of coarseness (a) 50; (b) 100; (c) 200, with black grains representing Titanium, and white grains representing Titanium Monoboride.

We carry out the numerical study on all the above model sizes using ABAQUS. The load applied is refined in such a manner that we can see the evolution of plastic grains in the microstructure. For the loading we applied, we are able to obtain plasticity of 25-27% in the microstructure for both boundary conditions. The contour plots for the von Mises stress for coarseness of 50 and 100 are shown in Figs. 3.12 and 3.13, respectively. We do not include the contours for coarseness of 200, as the results are visually fuzzy, and the shear bands are difficult to distinguish visually.

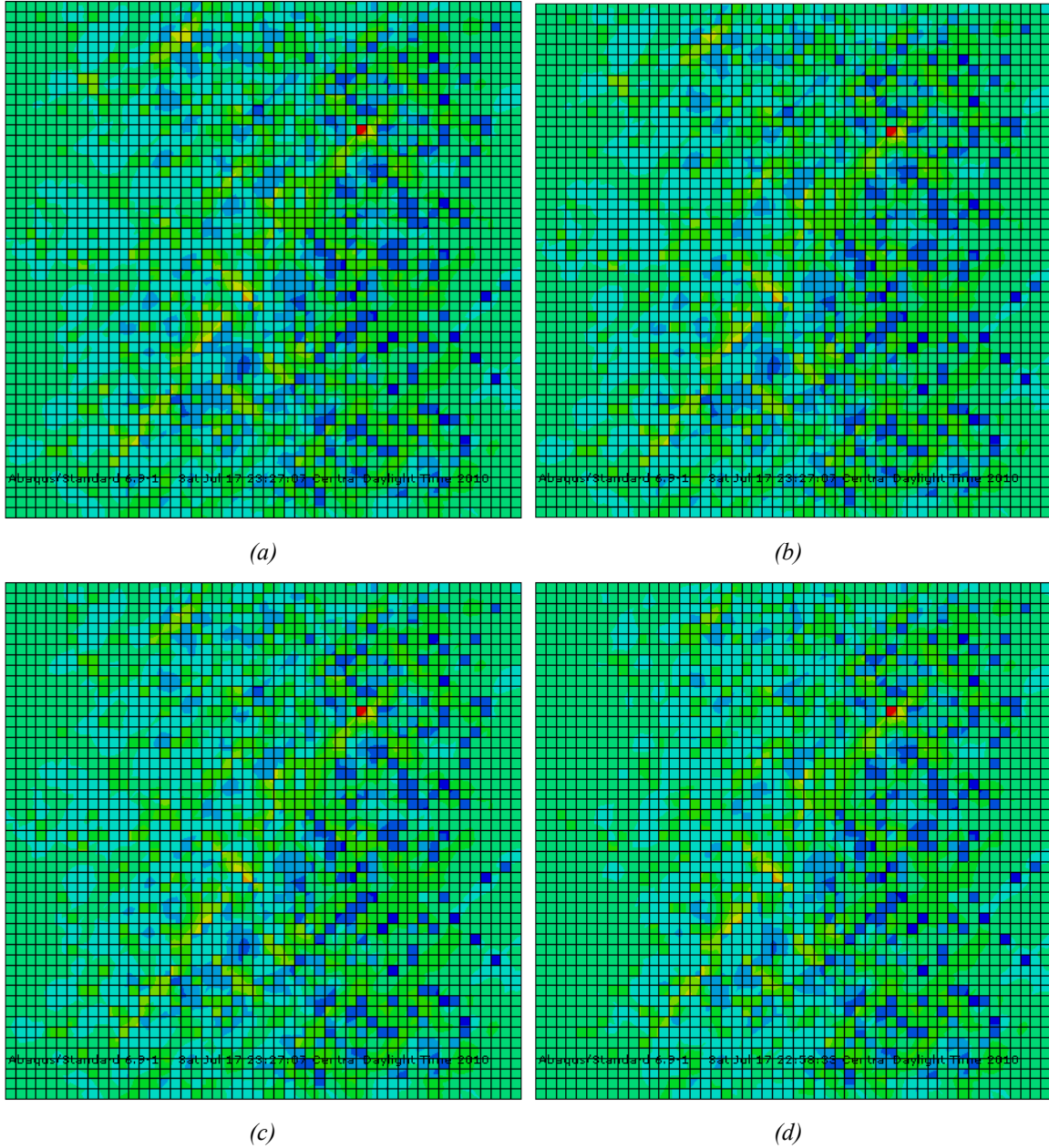


Figure 3.12 (a) Contour plot of von Mises stress for USBC at four different time instances for domain coarseness of

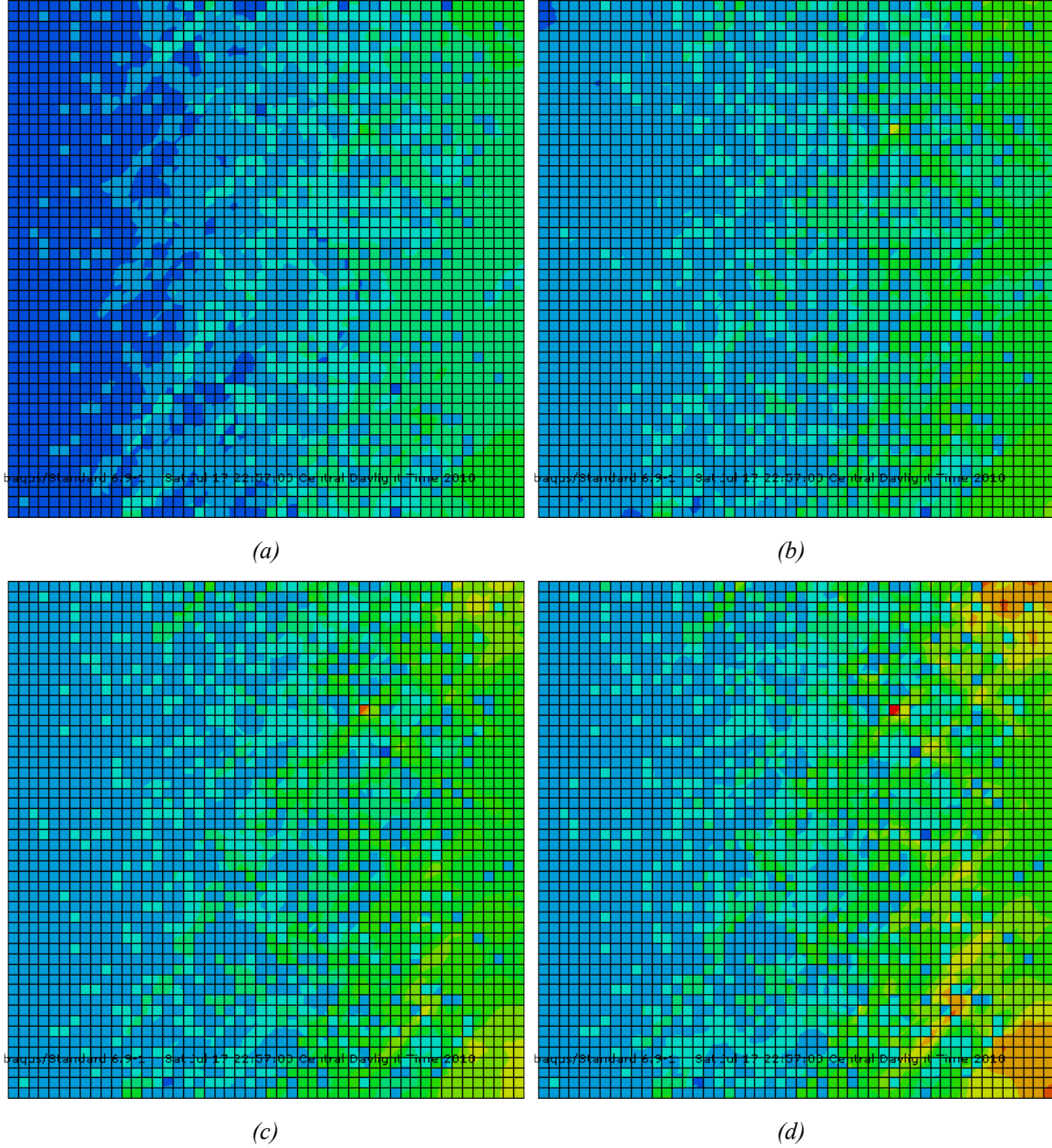


Figure 3.12 (b) Contour plot of von Mises stress for UKBC at four different time instances for domain coarseness of 50

We clearly see in Figs. 3.12(a) and (b) the formation of shear bands in the material due to the pure shear loading applied on the domain. These shear bands form in areas characterized by a high interfacial fractal dimension. We also notice this effect on the contour plots of coarseness of 100 in Figs. 3.13(a) and (b).

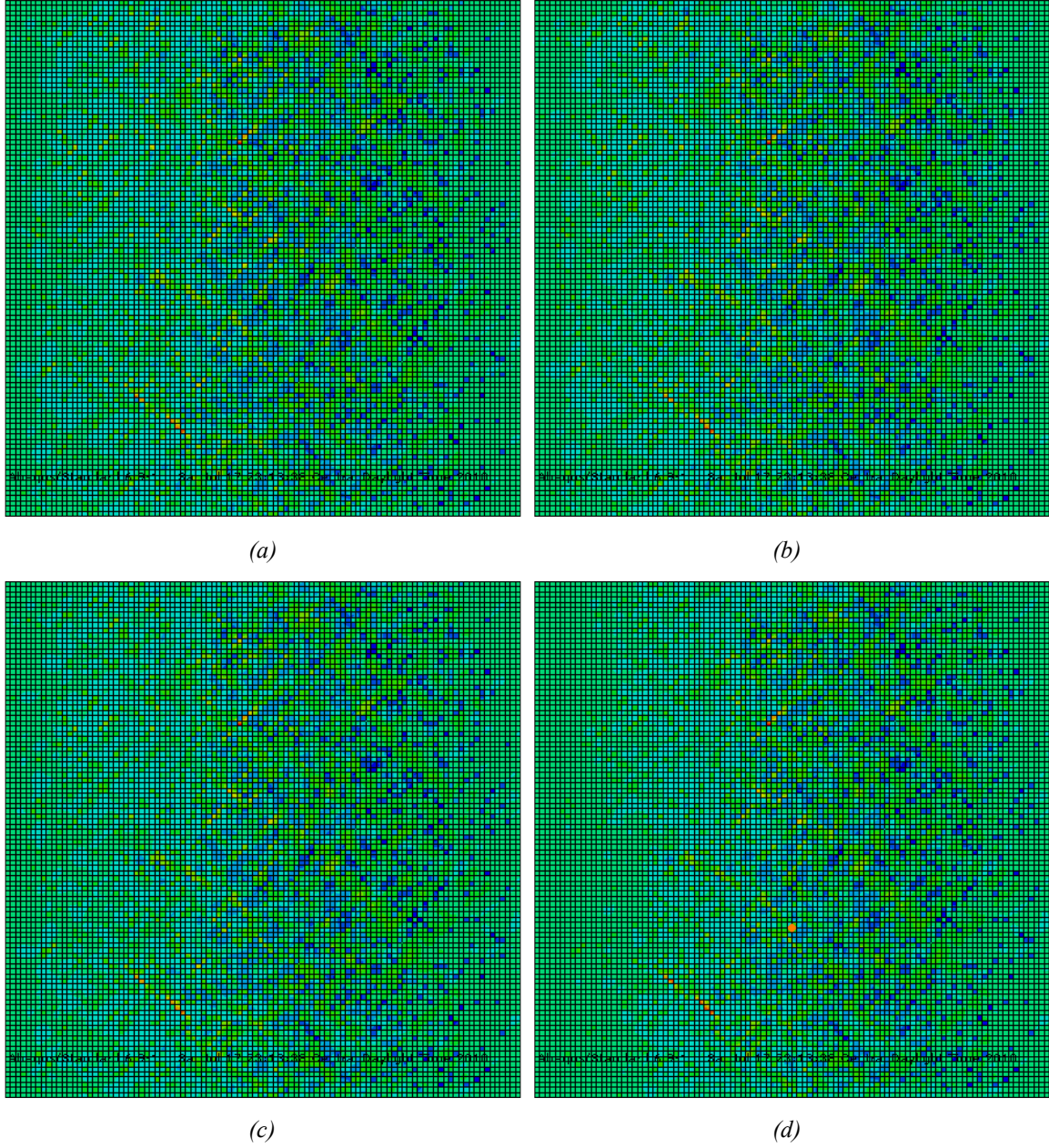


Figure 3.13 (a) Contour plot of von Mises stress for USBC at four different time instances for domain coarseness of 100



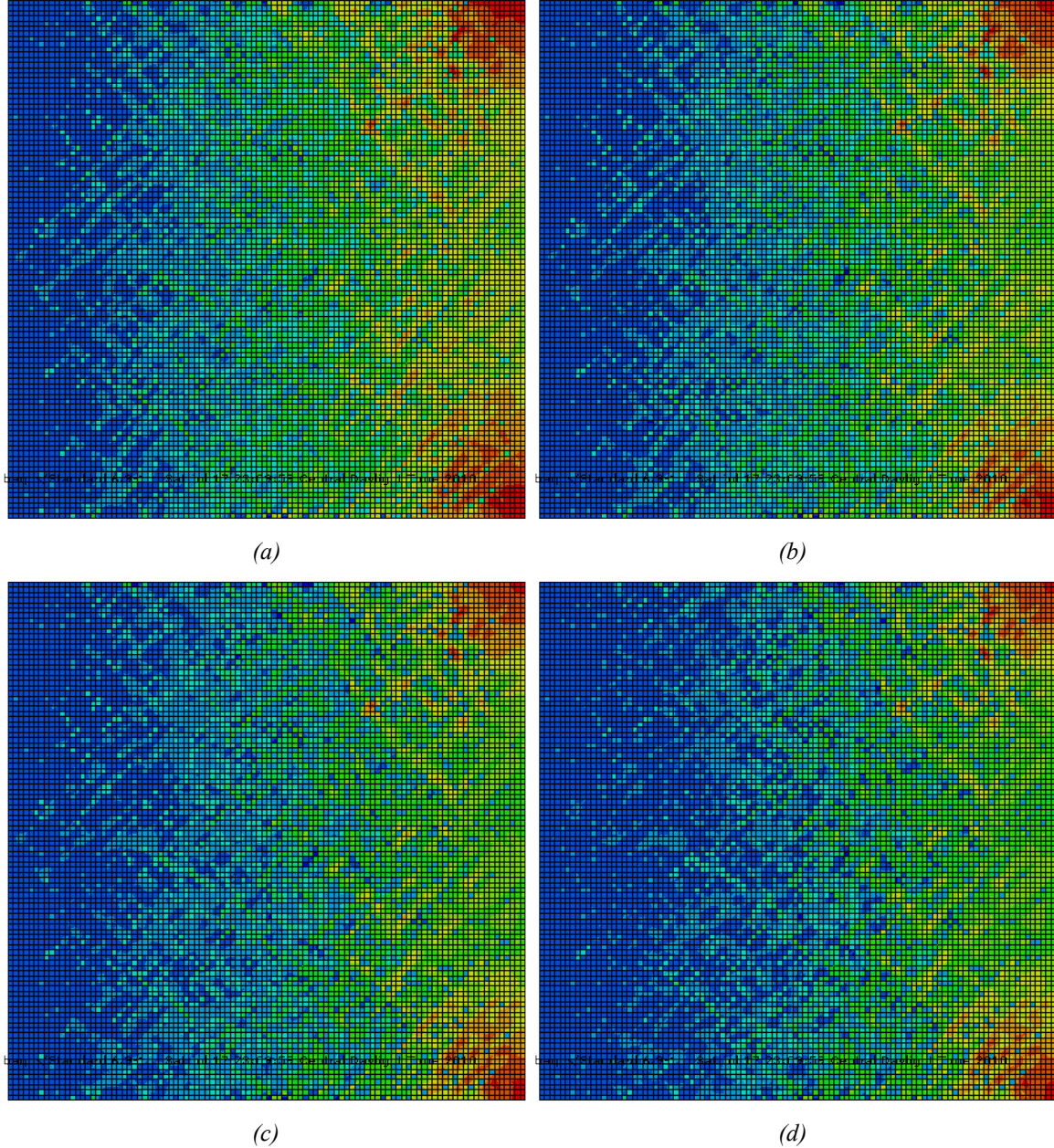


Figure 3.13 (b) Contour plot of von Mises Stress for UKBC at four different time instances for domain coarseness of 100

Furthermore, we observe from all the contour plots for all coarseness levels that shear bands form preferentially across regions having a rich Titanium-Titanium Monoboride (TiB) Interaction. However, these bands are not exactly at 45 degrees. Due to the heterogeneous nature of the FGM, the softer Titanium grains tend to grow plastic in such a way so as to avoid the stronger TiB grains. We also see some stress concentrations around the corners of the area rich in TiB under UKBC, which is understandable as the displacement applied at the boundaries leads to high stress levels in the TiB phase, as being a ceramic material it retains its elastic nature throughout.

Looking at our model, we now plot a volume averaged von Mises stress against a volume averaged plastic strain to check whether we can achieve the classical RVE response of the material. Figure 3.14 indicates this response curve for system coarseness of 50, 100 and 200.

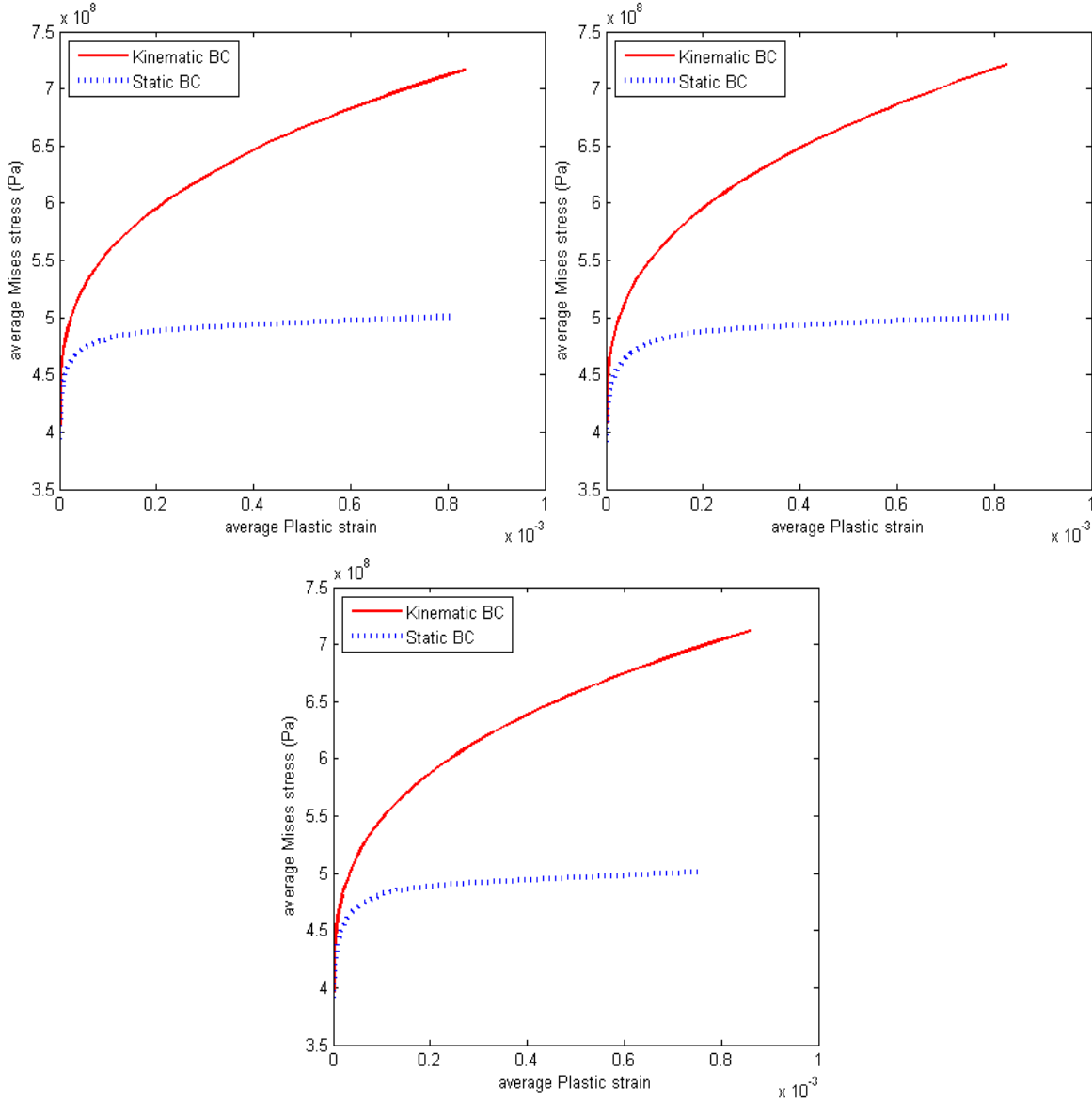
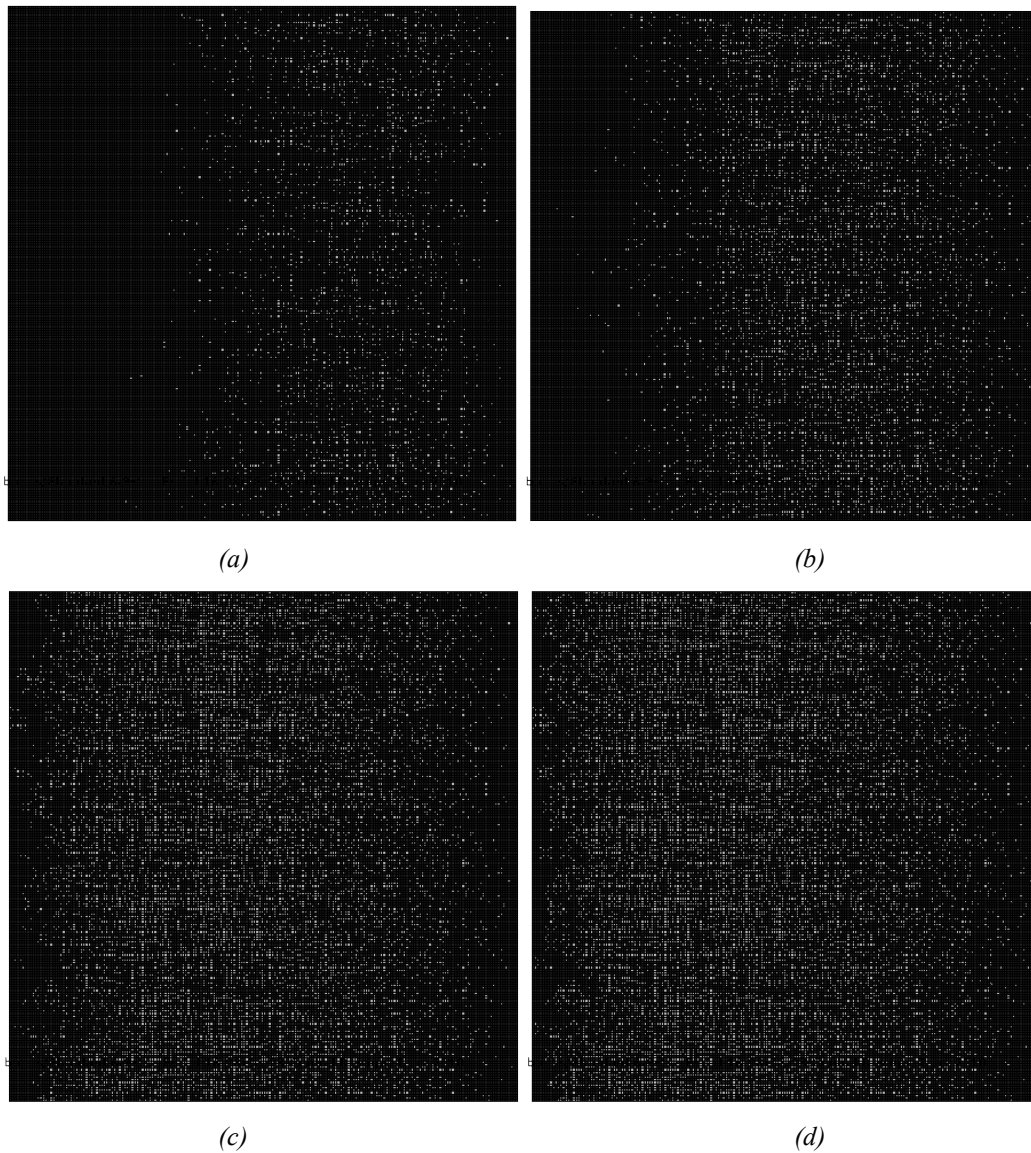


Figure 3.14 Volume Averaged Stress-Strain response under different BC's for coarseness of (from top left clockwise) (a) 50; (b) 100; (c) 200

As we can see from the plots given in Fig. 3.14, we fail to achieve constituent RVE response for our model under UKBC and USBC. Even as we increase the coarseness levels, or in other words refine our microstructure, we do not see any closing of the material response under the respective BC's. This could be reasoned out due to many reasons. Firstly, the USBC (traction) is very sensitive and often ill posed to elastic-plastic problems. Our calculations thus for plastic strain under this boundary condition is not reliable as it is underestimated due to lack of numerical efficiency of ABAQUS linear solver to

account for large plastic strains. Even if we could account for large plastic strains, the response would still not match the response under UKBC (displacement). Secondly, as our material is heterogeneous, with the TiB phase remaining elastic throughout, it does not reach high stress levels under USBC, even though the softer Ti phase continues to sustain large plastic strain due to plastic flow of the material. This indicates that our model is highly sensitive to the way it is loaded, and even a small change in loading conditions could elicit a varied response from the material.

We now turn our attention to formation of plastic grains (Ti grains) in our model under different boundary conditions. Evolution of Plastic grains under coarseness of 200 under UKBC and USBC is illustrated in Figs. 3.15 and 3.16 respectively.



*Figure 3.15 Evolution of Plastic Grains (White noise) under UKBC at four different time instances (starting top left) for coarseness of 200*



Looking at Fig. 3.15 we see that the growth of plastic grains of Titanium under UKBC starts towards the right side of the domain, which is a TiB rich region. This is understandable as uniform displacement on TiB boundary causes extremely high stress levels in TiB rich regions leading to plastic formation of Titanium grains in that region (represented by white noise in the above figure). As we move into the loading sequence, we observe that the plastic grains then slowly start evolving towards the Titanium rich regions on the left side of the domain.

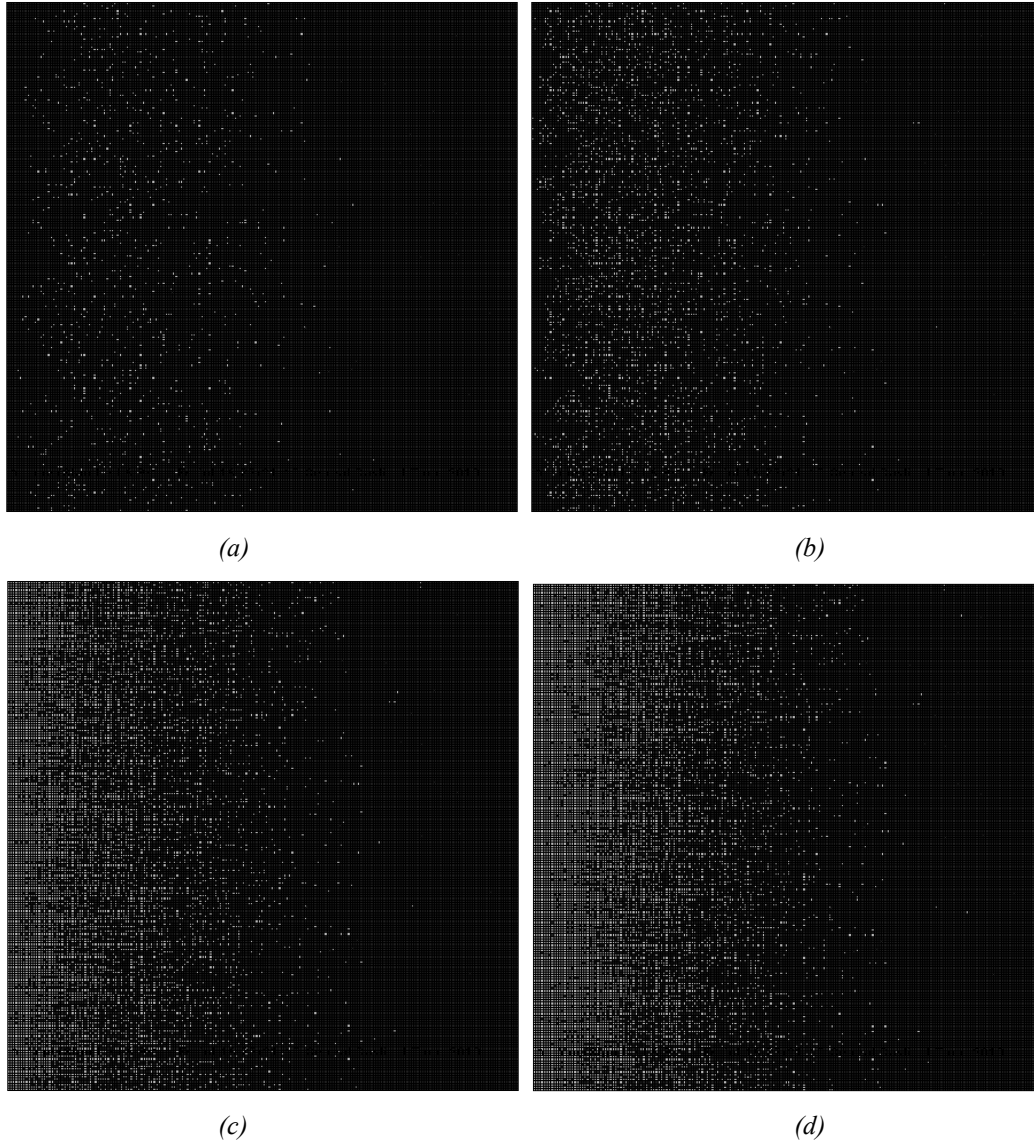


*Figure 3.16 Evolution of Plastic Grains (White noise) under USBC at four different time instances (starting top left) for coarseness of 200*

Now, looking at Fig. 3.16 we see the evolution of plastic grains (white noise) growing from Titanium rich regions (from the left). This can be reasoned as, under USBC leads to high stress levels in the Titanium rich regions, which leads to plastic flow in the material leading to plastic evolution of the

grains. As we proceed through the loading sequence, the plastic evolution of the Titanium grains starts progressing towards the middle of the system, with very few grains undergoing plastic deformation in the TiB region. This is because under USBC, the stress in TiB rich region doesn't reach levels high enough to cause plastic deformation of Titanium grains in the TiB rich region.

We can now estimate the fractal dimension  $D$  of the plastic grains evolving under both UKBC and USBC. It is done using the box counting method [14] for coarseness of 50, 100 and 200 at the end of the loading curve. The box counting method involves counting the number of boxes ( $Nr$ ) of a particular edge length ( $r$ ) required to cover the plastic grains in the entire domain. The plastic domain taken into consideration has plastic deformation ranging from 25% to 27% (for both boundary conditions) of the total 50%, which is the maximum plastic deformation for our model.

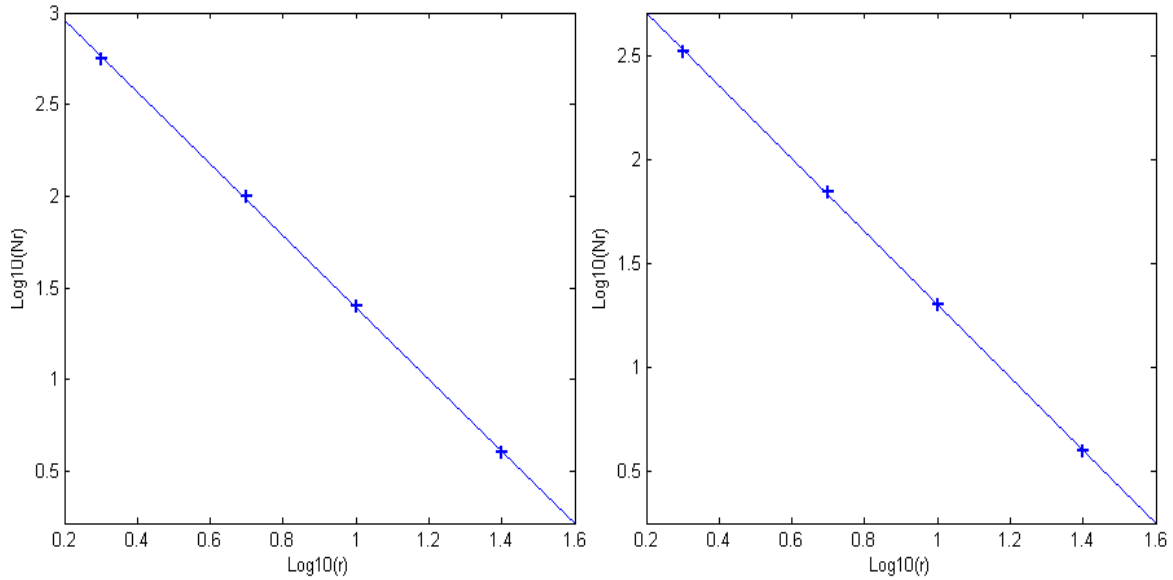


Figure 3.17 (from left) Estimation of the fractal dimension  $D$  using box counting for coarseness of 50 under (a) UKBC ( $D=1.9586$ ) and (b) USBC ( $D=1.7558$ )

In Fig. 3.17 we plot the log-log relationship between the number of boxes ( $Nr$ ) and the edge length of the box ( $r$ ), for both the boundary conditions. The fractal dimension for the UKBC and USBC is 1.9586 and 1.7558, respectively. The correlation coefficients in both cases were found to be very close to 1. The difference in the  $D$ , for both boundary conditions can be attributed to the plastic evolution of grains under respective boundary conditions as illustrated in Figs. 3.15 and 3.16, under UKBC, the plastic grains are more evenly distributed in the entire domain, and hence the higher  $D$  as compared to USBC where the plastic grains are mainly concentrated towards the Titanium rich region on the left side of the domain, hence the lower  $D$ . This validates our result of the mechanical testing of our model, where we found that the overall material response is extremely sensitive to the loading conditions.

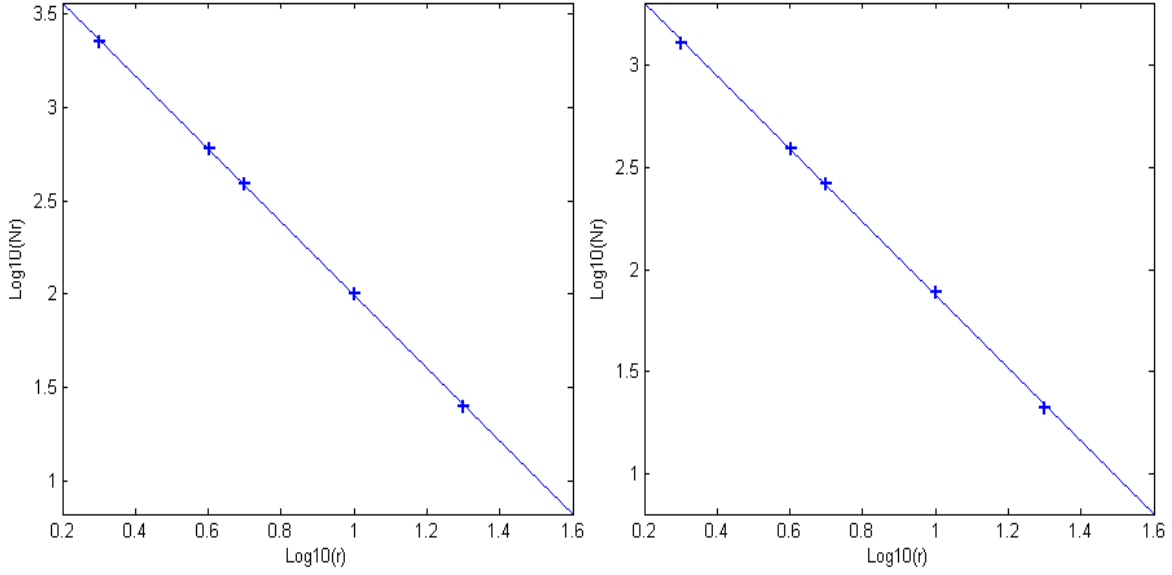


Figure 3.18 (from left) Estimation of fractal dimension  $D$  using box counting for coarseness of 100 under (a) UKBC ( $D=1.9555$ ) and (b) USBC ( $D=1.7837$ )

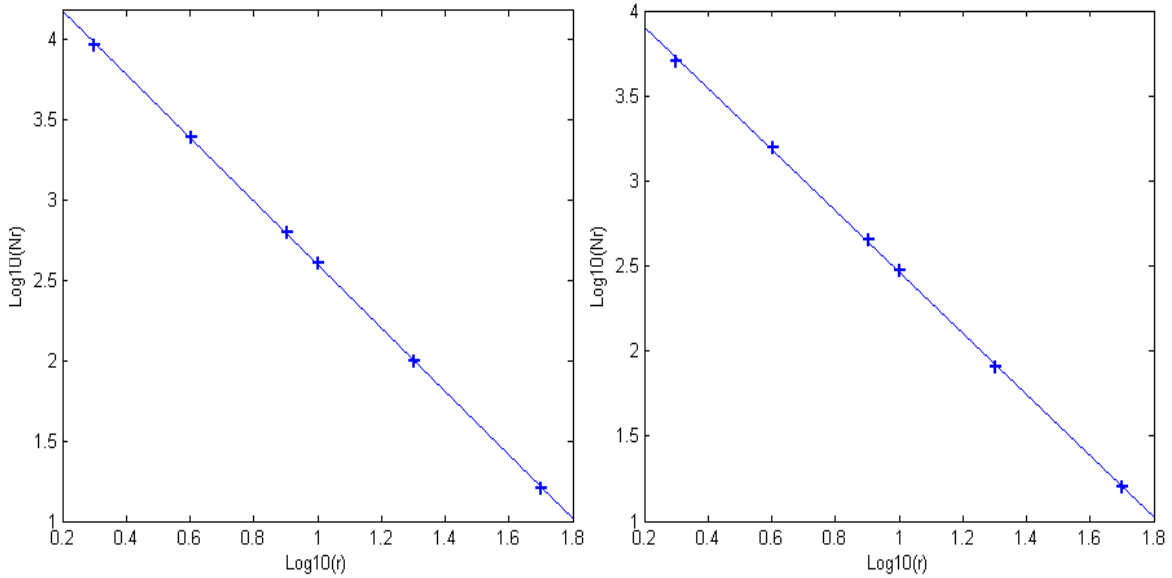


Figure 3.19 (from left) Estimation of fractal dimension  $D$  using Box counting for coarseness of 200 under (a) UKBC ( $D=1.9739$ ) and (b) USBC ( $D=1.7981$ )

We again plot the log-log relationship between the number of boxes ( $Nr$ ) and the edge length of the box ( $r$ ) for coarseness of 100 and 200 in Figs 3.18 and 3.19 respectively under both boundary conditions. The correlation coefficient as we can see from all the four plots has been estimated to be very close to 1.

The fractal dimension  $D$  for UKBC and USBC for all coarseness under consideration i.e. 50, 100 and 200 show little variation among themselves, and hence  $D$  can be a very useful parameter to estimate the plastic deformation for two-phase linearly graded FGM for both UKBC and USBC.

## CHAPTER 4 – CONCLUSIONS

We have setup a numerical model to study the Titanium and Titanium Monoboride (TiB) Functionally Graded Material System. That system has a piece-wise, one-dimensional geometry. The coarseness levels we have considered are of various degrees for both Geometrical Interpretation and Mechanical testing through the Finite Element Analysis. Referring to our both problem formulation setups in Chapter 2, we conclude the following.

- We generated FGM simulations on various coarseness levels ranging from 10 to 19,001. We then plotted the edge sets (interfaces between the black and white interfaces) and found them sparse near the boundaries and dense in the middle for each of our simulations. We then measured the interfacial fractal dimension in each simulation and observed a high noise in it for lower coarseness levels. Also, there is no trend seen in the variation of fractal dimension locally in the domain as we move widthwise (but not top-to-bottom) across the domain. However, we see a clear trend moving lengthwise (left to right) in the domain, which, in fact, can be characterized by a complicated relation given by a Fourier fit. A simple relation involving beta function can also be used to characterize the same, with both relations having comparable residuals.
- Mechanical testing was carried out using the commercial FEA package, ABAQUS. Titanium grains in the FGM were assumed to be isotropic elastically with isotropic plastic hardening. TiB grains in the FGM were assumed to be elastically isotropic throughout. By using both the UKBC and USBC, we applied pure shear loading on our model; it was observed that our model did not result in a classical constitutive RVE response. This means that the homogenization based on the Hill condition is extremely sensitive to the loading conditions. However, for both loading cases we achieved plasticity in the model ranging from 25% to 27%. We also observed that contour plots for von Mises stress for both loading conditions resulted in a formation of shear bands mainly across the regions having a high interfacial fractal dimension of the Titanium-TiB mixture.
- The plastic evolution of the Titanium grains under both boundary conditions displayed a fractal plane-filling behavior. The plastic grains under UKBC started evolving from the TiB rich region (containing some Titanium Grains) and spread towards the Titanium rich region progressing rather uniformly. Under USBC the plastic grains evolved mainly from the Titanium rich region and remained concentrated mainly in the same region. This fractal behavior was measured for both loading conditions using the box counting method. The fractal dimension showed little variation for each of the coarseness level under a particular boundary condition. However, the

fractal dimension under UKBC and USBC had different values. This validates our earlier result that the model response is highly sensitive to the loading conditions.

- The fractal geometry interpretation advanced in this thesis can be used to study the behavior of FGMs where the mismatch in properties across the interfaces of two phases are important - for example the heat transfer, electrical or magnetic conductivity, etc. The mechanical results show that the fractal dimension can be used to estimate the plasticity in a material for damage assessment in various mechanical equipment, presenting a good alternative to expensive strain gages, which require considerable amount of effort to install.
- This work can be further extended to test different material systems under anisotropic yield criteria. Also, it would be interesting to see the fractal behavior in 2D and 3D grading.

## BIBLIOGRAPHY

- [1] Miyamoto Y., Kaysser W.A., Rabin B.H., Kawasaki A., and Ford R.G., *Functionally Graded Materials: Design, Processing and Applications*.
- [2] Anandakumar Ganesh, Li Na, Verma Atul, Singh Prabhakar, and Kim Jeong-Ho, "Thermal stress and probability of failure analyses of functionally graded solid oxide fuel cells," *Journal of Power Sources*, vol. 195, 2010.
- [3] Gunes Recep and Aydin Murat, "Elastic response of functionally graded circular plates under a drop-weight," *Composite Structures*, 92 2010.
- [4] Hosseini Mahmoud Seyed and Shahabian Farzad, "Reliability of stress field in Al–Al<sub>2</sub>O<sub>3</sub> functionally graded thick hollow cylinder subjected to sudden unloading, considering uncertain mechanical properties," *Materials and Design*, vol. 31, 2010.
- [5] Feder Jens, *Fractals*. USA: Plenum Press, 1988.
- [6] Center for Engineering Research Inc., C-FIT User Guide.
- [7] Gasik Michael M., "Industrial Applications of FGM Solutions," *Material Science Forum*, vol. 423-425, 2003.
- [8] The American Ceramic Society. Ceramic Extrusion. [Online]. <http://ceramics.org/ceramictechtoday/tag/ceramic-extrusion/>
- [9] Lee Caroline S., Kim Sung-Geun, Ahn Sung-Hoon, DeJonghe Lutgard C., and Thomas Gareth, "Three Dimensional Analysis of Thermal Stress and Prediction of Failure of Polytypoidally Joined Si<sub>3</sub>N<sub>4</sub>-Al<sub>2</sub>O<sub>3</sub> Functionally Graded Material (FGM)," *MATERIALS TRANSACTIONS*, vol. 48, 2007.
- [10] Ishizuka T., Ohta Y., and Wakashima K., "Micromechanical failure criterion for FGM architecture studied via disk-bend testing of ZrO<sub>2</sub>/Ni composites.," *Composites*, 1996.
- [11] Shen Hui-Shen, "A comparison of buckling and postbuckling behavior of FGM plates with piezoelectric fiber reinforced composite actuators," *Composite Structures*, vol. 91, 2009.
- [12] Nemat-Alla Mahmoud, Ahmed Khaled I.E., and Hassab-Allah Ibraheem, "Elastic–plastic analysis of two-dimensional functionally graded materials under thermal loading," *International Journal of Solids and Structures*, vol. 46, 2009.
- [13] Aboudi Jacob, Pindera Marek-Jerzy, and Arnold Steven M., "THERMO PLASTICITY THEORY FOR BIDIRECTIONALLY FUNCTIONALLY GRADED MATERIALS," *Journal of Thermal Stresses*, vol. 19, 1996.

- [14] Li Jun and Ostoja-Starzewski M., "Fractal Pattern Formation at Elastic-Plastic Transition in Hetrogeneous Materials," *Journal of Applied Mechanics*, vol. 76, November 2009.
- [15] Li Jun and Ostoja-Starzewski M., "Fractals in elastic-hardening plastic materials," *Proc. Roy. Soc. Lond. A*, 2009.
- [16] Bhandari D.R. and Oden J.T., "A LARGE DEFORMATION ANALYSIS OF CRYSTALLINE ELASTIC-VISCOPLASTIC MATERIALS," *NUCLEAR ENGINEERING AND DESIGN*, vol. 29, 1974.
- [17] ULBRICH. [www.ulbrich.com](http://www.ulbrich.com).
- [18] Welsch Gerhard, Boyer Rodney, and Collings E.W., *Materials properties handbook: titanium alloys.*: ASM International, 1994.
- [19] Atri R.R., Ravichandran K.S., and Jha S.K., "Elastic properties of in-situ processed Ti-TiB composites measured by impulse excitation of vibration," *Materials Science and Engineering*, vol. A271, 1999.
- [20] Madtha Shawn, Lee Curtis, and Ravichandran K. S., "Physical and Mechanical Properties of Nanostructured Titanium Boride (TiB) Ceramic," *J. Am. Ceram. Soc.*, vol. 91, 2008.
- [21] PANDA K.B. and RAVICHANDRAN K.S., "Titanium-Titanium Boride (Ti-TiB) Functionally Graded Materials through Reaction Sintering: Synthesis, Microstructure, and Properties," *METALLURGICAL AND MATERIALS TRANSACTIONS A*, vol. 34A, 1993.
- [22] Panda K.B. and Ravichandran K.S., "First principles determination of elastic constants and chemical bonding of titanium boride (TiB) on the basis of density functional theory," *Acta Materialia*, vol. 54, 2006.
- [23] Larson Reid A., "A Novel Method For Characterizing the Impact Response of Functionally Graded Plates," Air Force Institute of Technology, Dissertation 2008.
- [24] Saito Takashi, *The Automotive Application of Discontinuously Reinforced TiB-Ti Composites*, 2004.
- [25] Biswas Prasad Chandi, "Strain hardening of titanium by severe plastic deformation," Massachusetts Institute of Technology, Doctoral Thesis 1973.